ELSEVIER

Tectonophysics 343 (2001) 205–232

TECTONOPHYSICS

www.elsevier.com/locate/tecto

Estimating slip rates and recurrence intervals for strong earthquakes along an intracontinental fault: example of the Pambak–Sevan–Sunik fault (Armenia)

Hervé Philip [a,*], Ara Avagyan [a], Arcadi Karakhanian [b], Jean-François Ritz [a], Samira Rebai [a]

[a] *Laboratoire de Géophysique, Tectonique et Sédimentologie, UMR 5573, Université Montpellier II, Place Eugène Bataillon, 34095 Montpellier Cédex 05, France*

[b] *"Georisk" Scientific Research Company, 24a Bagramyan, Yerevan 375019, Armenia*

Received 25 February 2000; accepted 24 October 2001

Abstract

North of the Arabian plate, active tectonics is characterised by both N–S compression and E–W extension associated with strike-slip faults. The Pambak–Sevan–Sunik fault (PSSF) zone in Armenia is one of the major active structures of the region. The fault is comprised of four main segments and it displays morphological evidence for dextral movement during the Holocene. However, no large earthquake ($M > 7$) has occurred in the northern or central parts of the fault during the last 2000 years. We undertook a geomorphological and paleoseismological investigation along the Pambak–Sevan–Sunik fault with the aim of estimating the long-term slip rate and recurrence interval of strong earthquakes. Trenches were excavated at three sites. Detailed studies of trench cross sections and dating (radiocarbon and ceramics) show three faulting events that occurred in the Vanadzor–Artanih segment (Fioletovo and Semionovka areas), whereas a single event took place in the Artanish–Sunik segment (Khonarhasar area). In both areas, we estimated the average slip rate using (i) the offset of rivers along the Vanadzor–Artanish segment (2.24 ± 0.96 mm/year over an interval of 120–300 ka), and (ii) the offset of volcanic cones along the Artanish–Sunik segment (0.53 ± 0.04 mm/year over an interval of 1.4 Ma). These results suggest that a greater slip rate characterises the Vanadzor–Artanish segment (Fioletovo site) from the Artanish–Sunik (Khonarhasar site) segment. Division of the Pambak–Sevan–Sunik fault zone into two main branches, east of the Artanish peninsula (Sevan Lake) could explain the difference in slip rate. In addition to its segmented seismic behaviour, the Pambak–Sevan–Sunik fault is a well-documented example of a fault that generates strong earthquakes with long recurrence time intervals (about 3000–4000 years).

Keywords: Active tectonics; Paleoseismology; Earthquakes; Caucasus; Armenia

1. Introduction

The Great and Lesser Caucasus Mountain ranges and the highly elevated region of the Armenian upland constitute a segment of the Alpine fold belt.

* Corresponding author.
E-mail address: philip@dstu.univ-montp2.fr (H. Philip).

0040-1951/01/$ - see front matter
PII: S0040-1951(01)00258-X

Many authors (Ketin, 1948; McKenzie, 1972; Sengör and Kidd, 1979; Jackson and McKenzie, 1984; Dewey et al., 1986; Taymaz et al., 1991) agree to relate their formation to the northward motion of the Arabian plate with respect to Eurasia, at a rate estimated at 20–30 mm/year (De Mets et al., 1990). As a consequence of this convergent movement, the Anatolian and Iranian blocks were pushed to the west and the east respectively, while the central region experienced intense shortening. The latter area is marked by intense seismic and volcanic activity (Fig. 1). Relatively complex active tectonics, characterised by both N–S compression and E–W extension, is associated with Neogene to Quaternary volcanism (Rebaï et al., 1993). This volcanic activity is one of the most remarkable features of a large area extending from East Anatolia to Central Iran.

In eastern Anatolia, western Iran, Armenia and the Caucasus, numerous active strike-slip and reverse faults form large structural wedges bounded by dextral slip on the eastern flank and sinistral slip on the western flank. The wedges fit into each other, with tips oriented to the north and northeast (Fig. 1). The Daghestan, North Armenian and Talish wedges are the largest (Fig. 1). Deformation within the wedges is characterised by (i) east–west folding and thrust faults, (ii) oblique strike-slip, and (iii) north–south normal faults with volcanic activity oriented parallel to the shortening direction (Philip et al., 1989; Rebaï et al., 1993; Karakhanian et al., 1996).

Previous studies based on the estimated sum of the seismic moment of earthquakes (Kostrov, 1974; Molnar, 1979) provided an average value of 1.3 mm/year for the shortening rate in this section of the Alpine belt

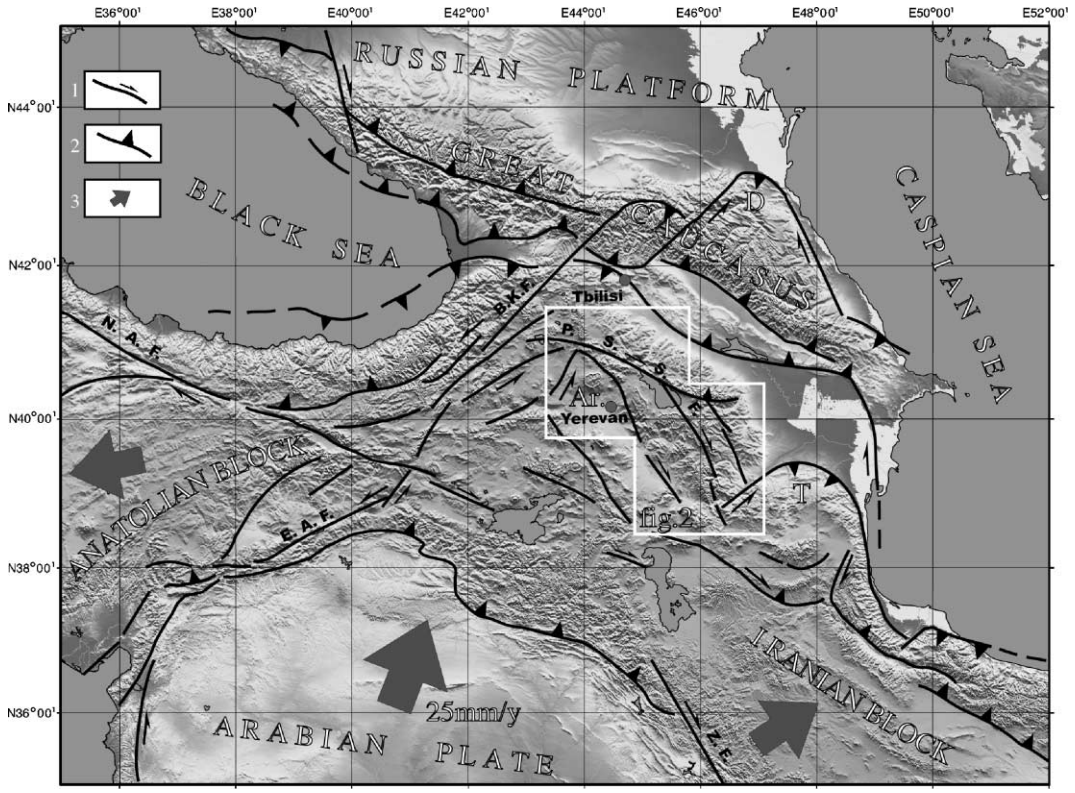

Fig. 1. Active tectonics north of the Arabian plate (after Philip et al., 1989; Rebaï et al., 1993). (1) Major strike-slip faults; (2) major thrust faults; (3) relative motion of blocks with respect to Eurasia. Ar — Armenia; D — Dagestan; T — Talish; E.A.F. — East Anatolian fault; N.A.F. — North Anatolian fault; P.S.S.F. — Pambak – Sevan – Sunik fault; Z.F. — Zagros fault.

(Philip et al., 1989; Jackson, 1992). Compared with the Arabian–Eurasian convergence rate, which is estimated at 20–30 mm/year, the average shortening value suggests that 80–90% of the deformation is aseismic (Chase, 1978; Minster and Jordan, 1978; De Mets et al., 1990).

Recent GPS data obtained across this region of crustal shortening allows us to fix the upper limit of the regional strain rate at 10 ± 2 mm/year. (Reilinger et al., 1997). Because such a rate cannot account for aseismic slip or permanent deformation of the blocks bounding the fault, this value also represents an upper limit for the elastic strain accumulation rate. Moreover, the same authors also report geodetic recurrence intervals of about 400 years for M 6.5 earthquakes on bounding thrust faults of the Lesser and Greater Caucasus, which reflects a lower limit for present-day recurrence intervals. These recurrence times estimated from GPS measurements are less than that determined from historical earthquakes or paleoseismological data (about a factor two for the North Anatolian Fault and probably more for other regions in the Middle East, according to Reilinger and Barka, 1997). The authors have put several explanations forward to explain this apparent discrepancy. Underestimating the total number of faults accommodating deformation in the region is one of these reasons. This seems an important factor to us.

The zone studied extends from eastern Anatolia to western Iran and includes all of the Armenian uplands. It is characterised by a high level of seismic activity. Abundant historical information indicates that the region has experienced strong earthquakes, many of which occurred along large-scale active fault zones. The strongest recorded earthquakes (Fig. 2) appear to have occurred on the North Tabriz (1042, $M=7.6$; 1721, $M=7.7$; 1780, $M=7.7$), the Balik–Gel (550 B.C., $M=7.0$; 1840, $M=7.4$), the Garni (906, $M=7.0$; 1679, $M=7.0$) and the Pambak–Sevan–Mrav faults (1139, $M=7.5$) (Ambraseys and Adams, 1989; Ambraseys and Melville, 1982; Shebalin and Tatevossian, 1997; Berberian, 1995; Karakhanian et al., 1997).

The earthquakes of Chaldiran (eastern Turkey, 1976, $M=7.1$), Spitak (Armenia, 1988, $M=7.0$) and Racha Dzava (Georgia, 1991, $M=7.0$) were the strongest regional seismic events in recent times (Ambraseys, 1988; Philip et al., 1992; Trifonov et al., 1990).

Instrumental seismicity is mainly represented by scattered shallow events of moderate size that tend to concentrate along the main active fault zones, in particular north of the front of tectonic wedges, thus within tectonic extension sites (Philip et al., 1989; Rebaï et al., 1993; Karakhanian et al., 1997).

While reliable instrumental and historical seismicity data are available for the region, there exists no paleoseismological data, with the exception of that of the Spitak fault, which was collected shortly after the 1988 Spitak earthquake (Philip et al., 1992). However, many active faults provide reliable geomorphological evidence of Holocene deformation along the northern and central parts of the Pambak–Sevan–Sunik fault (PSSF).

2. The Pambak–Sevan–Sunik fault

Our studies have been carried out in conjunction with detailed analysis of air photos and SPOT and Landsat-TM satellite imagery, and the computation of numerical relief models based on detailed topographic maps (Digital Elevation Models). Tectonic, seismotectonic and paleoseismological studies were accomplished during the field campaigns of 1996, 1997, 1998 and 1999. In 1989–1990 and 1993–1994, preliminary studies were done on individual fault sites within the 1988 Spitak earthquake region (Philip et al., 1992; Trifonov et al., 1990) and in Sunik area (Karakhanian et al., 1997). The results of these studies have provided first-order data on the geometry, kinematics, slip rates, seismic potential and strong earthquake recurrence intervals along the PSSF system.

The PSSF joins other active faults (Geltareshka–Sarikhamich, Akhurian and Garni faults) to the north–west. Together they form the North Armenian tectonic wedge. The extensional zone of the Javakhet volcanic massif is located north of this wedge (Figs. 1 and 2).

The PSSF corresponds to a large active structure that bounds the North Armenian structural wedge to the east (Figs. 1 and 2). This fault extends north–west to south–east and splits into three branches in the Artanish Cape area: Mrav, the northern branch, Akerin, the central branch, and Sunik, the southern branch. In

this paper, we discuss the southern, namely PSS, branch of this system.

The PSSF system is clearly identified on topographic maps and by field geomorphology and can be traced continuously along 400 km. This fault system consists of four major segments (Fig. 2) separated by step-over zones:

1. 88-km-long Arpi–Vanadzor segment striking 105° (1, Fig. 2);

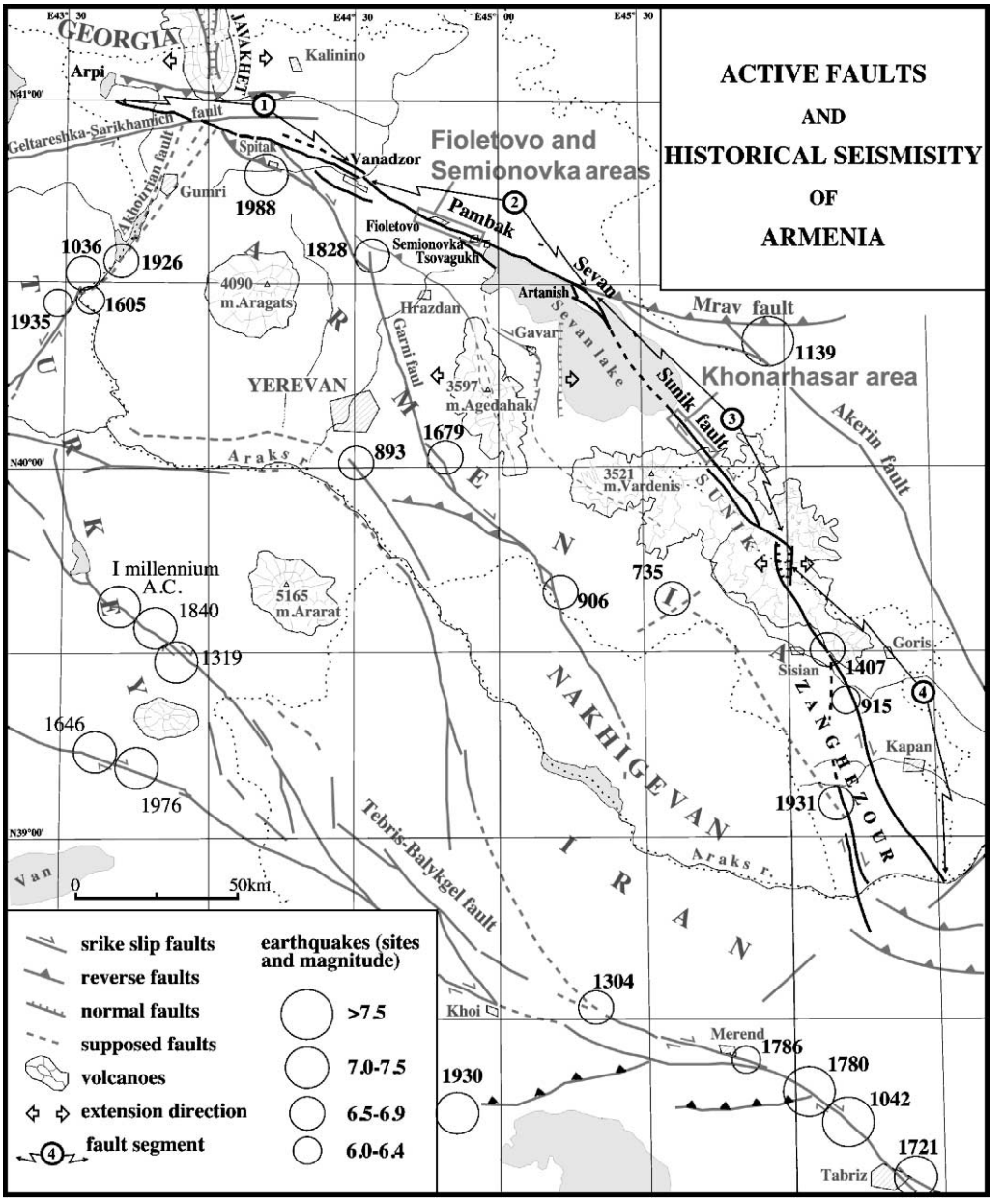

Fig. 2. Main active faults and historic seismicity of Armenia. Numbers adjacent to epicentres are dates of earthquakes (in years A.D.). The four segments of the PSSF are labelled: (1) Arpi–Vanadzor, (2) Vanadzor–Artanish, (3) Artanish–Sunik, and (4) Sunik–Zanghezour.

2. 90-km-long Vanadzor–Artanish segment striking 115° (2, Fig. 2);
3. 110-km-long Artanish–Sunik segment of more oblique 142° strike (3, Fig. 2);
4. 120-km-long Sunik–Zanghezour segment striking 155° (4, Fig. 2).

Dextral strike-slip movements are observed along the entire length of the PSSF. They are often associated with vertical (mainly reverse) displacements that can be clearly identified on satellite images, air photos and topographic maps. Cumulative horizontal displacements of 1.8 km (young tributaries) to 3 km (major valleys) are recorded along the western fault segments (Rebaï et al., 1993; Trifonov et al., 1990).

A large pull-apart basin formed at the junction of the Artanish–Sunik and Sunik–Zanghezour segments. Surface ruptures from a large pre-historic earthquake are observed within this pull-apart. This faulting event was accompanied by a volcanic eruption with basaltic lava flows overlying petroglyphs (Karakhanian et al., 1997).

Historical seismicity data (Fig. 2) give evidence for the activity of the southeastern Sunik–Zanghezour

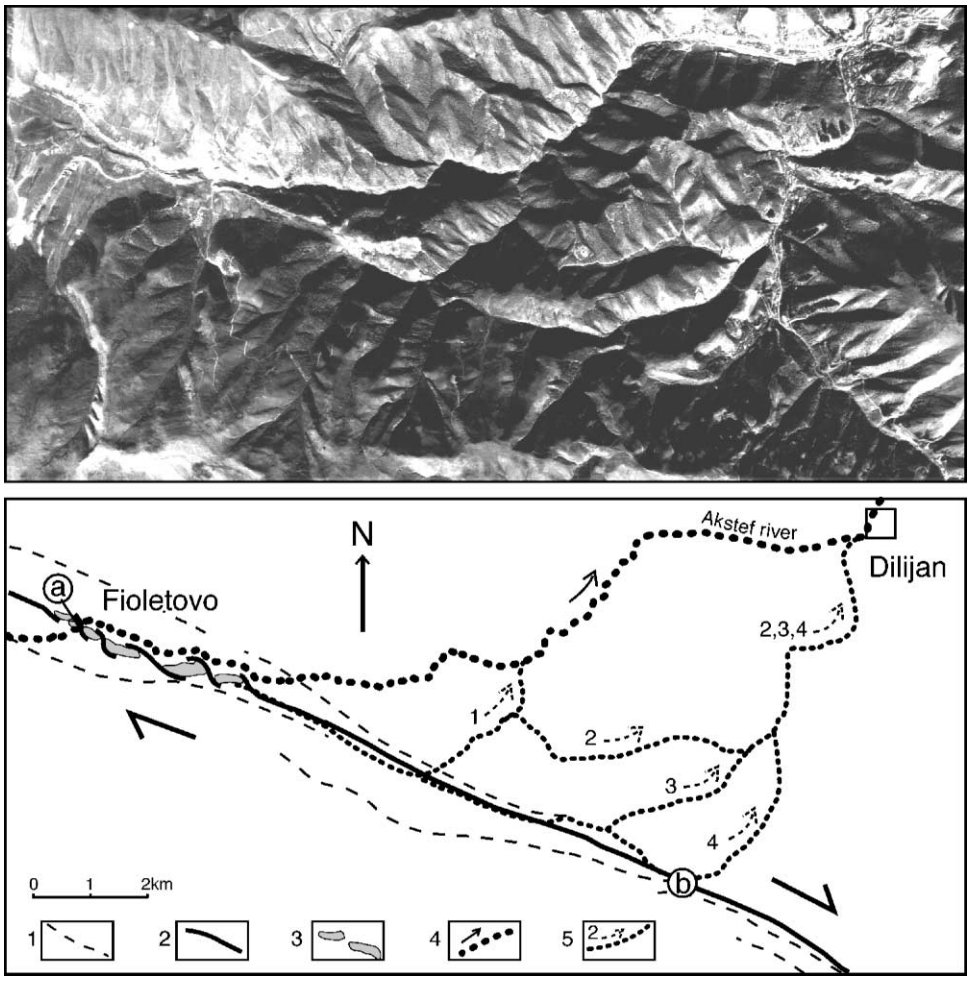

Fig. 3. Drainage evolution of the Akstef River during the Late Quaternary. (1) Inactive fault segments; (2) active fault segments; (3) en-échelon hills; (4) modern Akstef River; (5) abandoned valleys of the Akstef River (1 is the youngest, 4 is the oldest).

segment, the site for the earthquakes of 915 ($M=6.0$), 1407 ($M=7.0$) and 1931 ($M=6.4$). Two historical earthquakes with an estimated magnitude of less than 6 occurred in the north–west of the Sevan Lake in 1187 ($M=5.5$) and 1853 ($M=4.5$).

3. Spot image and air-photo analysis combined with field data and paleoseismological investigations

We focused our study of the PSSF zone on three main regions that proved ideal for the analysis of active tectonics and paleoseismicity and the determination of slip rate.

3.1. The Fioletovo and Semionovka areas

3.1.1. Geologic and geomorphic setting

Two of the selected sites, Fioletovo and Semionovka, respectively, are located within the Vanadzor–Artanish segment of the fault zone (Fig. 2). The over-stepping fault segment creates three major jog-type structures with their inner parts depressed in the areas of the towns of Vanadzor, Fioletovo and Tsovagukh along the western bay of the Sevan Lake.

Satellite images and air photos show a system of elongated ridges in a dextral en échelon pattern along the axis of the Fioletovo depression. These ridges clearly appear as scarps on topographic maps and in the field (Figs. 3 and 4). The ridge axes have an average length of between 100 and 1500 m, while minor ridges have axis lengths of 30–500 m. The ridge heights vary between 5–6 and 30–50 m. A similar system of ridges, interpreted as pressure ridges, can also be identified in the Vanadzor depression, as well as in the northern boundary and the central part of the Sevan depression. In many cases, the ridge flanks are very steep (50°–60°) and show well-preserved evidence for young scarps.

In the Semionovka site (Fig. 5), elongated ridges located along the trace of the PSSF are interpreted as counter slope scarps associated with south-dipping reverse faults. The length of the ridge axes varies between 50 and 800 m. The misalignment of thalwegs suggests a dextral displacement, which is consistent with the oblique dextral movement observed on the fault plane.

3.1.2. Estimation of the slip rate

Numerous right-lateral offsets of the river network and small ravines can be observed along the entire length of the zone studied. In SPOT and air-photo images, an abandoned valley system of the Akstef River is clearly seen east of Fioletovo (Fig. 3). Right-lateral strike-slip displacements, along with vertical uplift of the northern fault block resulted in a stage-by-stage overlap (interception) of the Akstef riverbed, with sequential migration of its abandoned valleys to the east. The fact that the abandoned valleys are part of the old Akstef river system is supported by their very deep

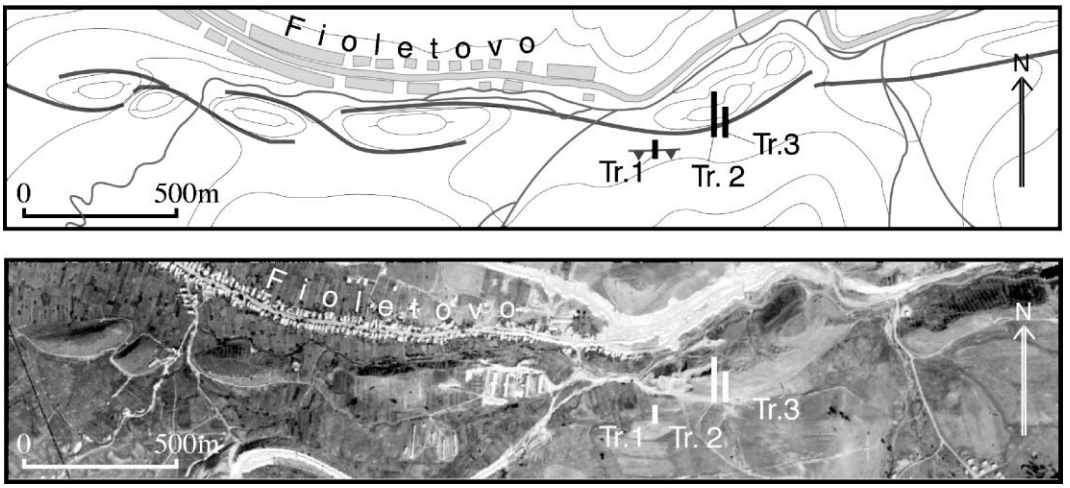

Fig. 4. Ridge alignment and trench locations in the Fioletovo site.

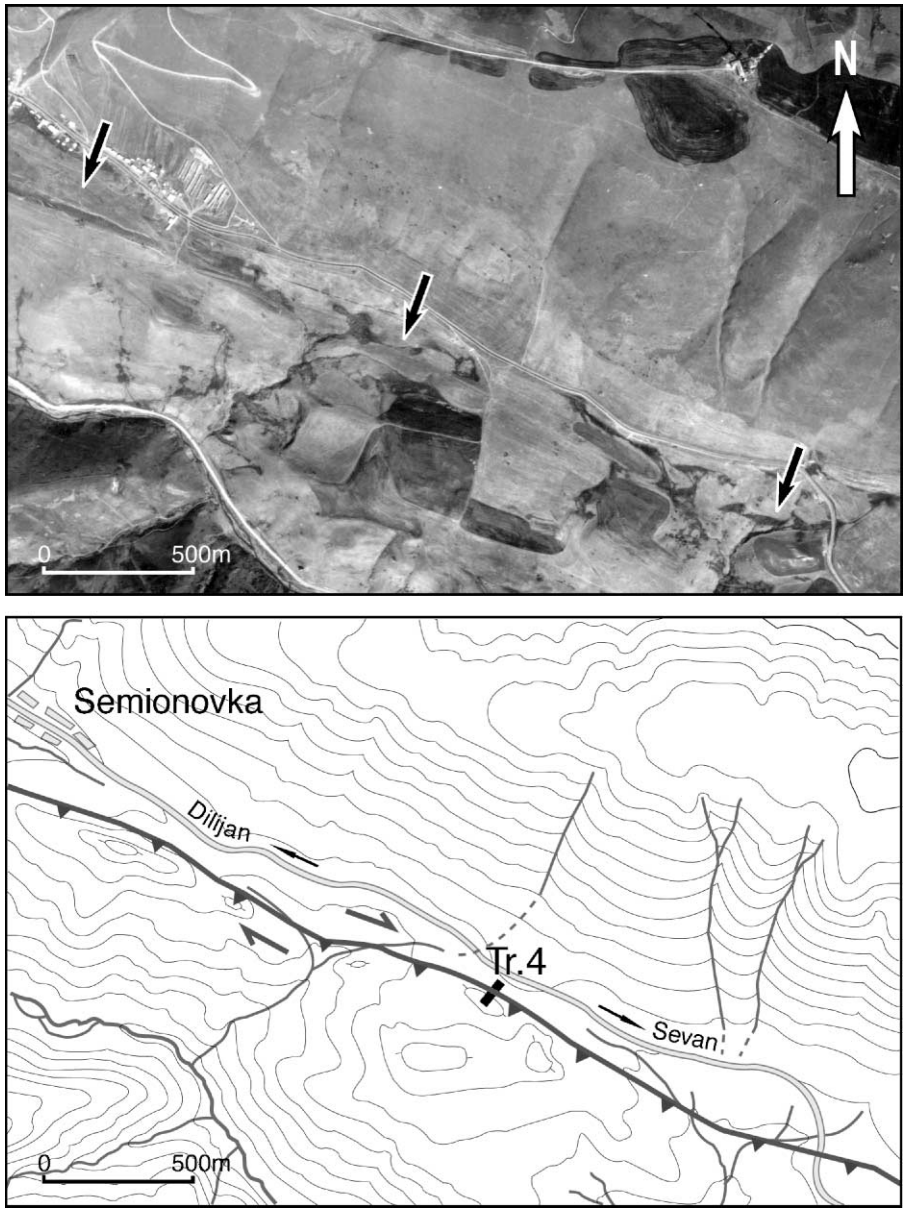

Fig. 5. Ridge alignment and trench locations in the Semionovka site.

erosive incision, when compared to the surrounding river network, and by the absence of other possible feeding basins. Based on the air-photo interpretation, four generations of riverbeds can be identified (no. 1 being the most recent and no. 4 the oldest). Dextral stream misalignment observed in the oldest riverbed reaches up to 8 km, but it is difficult to estimate the amount due to tectonic translation. On the other hand, the difference in elevation between points a and b (Fig. 3) of the thalweg is 220 ± 5 m, which provides a more reliable way for calculating the vertical slip rate. The age of the oldest paleo-valley (4 in Fig. 3) needs to be evaluated to estimate the uplift rate. The oldest fluvio-glacial terraces along the Pambak River, equiv-

alent and close to the Akstef River, are Riss in age (i.e. 300,000–120,000 years BP) (Vardaniants, 1948). Using these values, the vertical uplift rate for the Vanadzor–Artanish fault segment can be estimated at 1.29±0.57 mm/year. A 30° rake of striation was measured along the Pambak–Sevan fault in two places: (i) at a nearby site West of Fioletovo, and, (ii) in Trench IV near the village of Semionovka. This value allows us to estimate the rate of horizontal displacement along the Vanadzor–Artanish fault segment. For 220±5 m of vertical displacement, there should be 381±8.6 m of horizontal offset, which yields a horizontal slip rate of 2.24±1 mm/year. The estimated slip rate represents a maximum value since erosion of the paleo-valley could have occurred before the Riss age.

3.1.3. Paleoseismological investigation

To characterise the paleoseismic activity along the Vanadsor–Artanish fault section, three trenches were excavated near the village of Fioletovo (Trenches I, II and III in Fig. 4) and one near the village of Semionovka (Trench IV in Fig. 5). They were excavated at the foot of the southern slope of the largest ridge (Figs. 4 and 6), located a few hundred meters east of Fioletovo, and on the northern slope of a ridge located 1.5 km east of Semionovka. Trench II will not be described in detail in this study, because nearby Trench III (Fig. 6) is the deepest and displays more information.

3.1.3.1. Trench I. Trench I is the smallest excavated trench. It was excavated in 1996 on a secondary scarp (Figs. 4 and 7) about 20 m south of the main pressure ridge.

3.1.3.1.1 Stratigraphy, sedimentary environment and structures. A log of this trench (mapped in the field at the 1:20 scale) is shown in Fig. 7. Six main sedimentary units have been identified from the bottom to the surface:

(1a) Homogeneous and well-compacted layer of grey plastic clay;
(1b) Homogeneous layer of yellow clay;
(1aA–1bA) Paleosol layer, 10 cm in thickness that developed on units 1a and 1b containing centimetresized limestone clasts. The matrix of this unit consists of silt with abundant organic fractions.

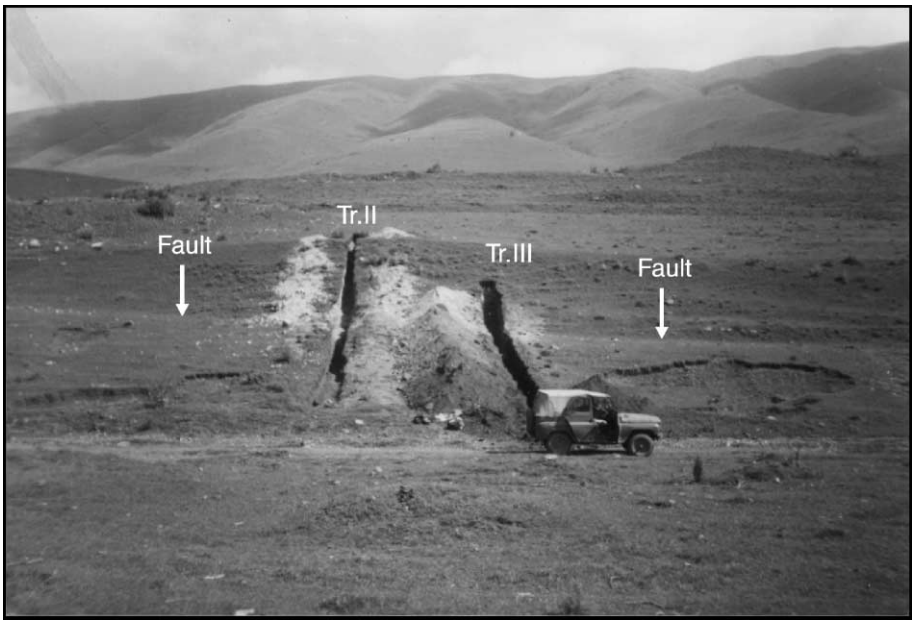

Fig. 6. Trenches II and III in 1997.

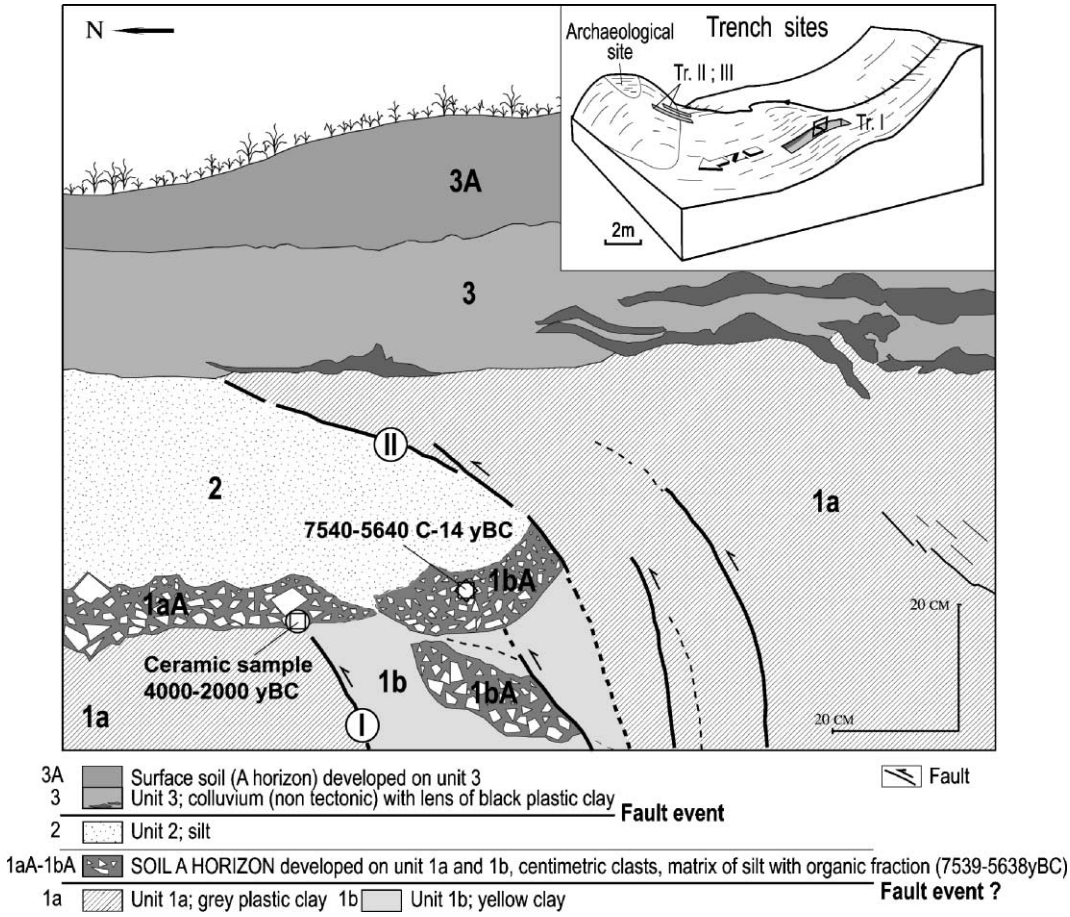

Fig. 7. Log of Trench I.

Ceramic fragments indicate that human activity was associated with its formation.

(2) Silt layer that overlies the paleosol.

(3) Colluvium composed of limestone pebbles in a matrix with abundant organic material and lenses of black plastic clay.

(3A) Modern soil.

Several fault planes dipping to the south are present. Their dip increases with depth until the faults become sub-vertical. The northern fault (I, Fig. 7) is buried by the paleosol level (1aA–1bA). The main fault (II, Fig. 7) cuts across both the paleosol (1aA–1bA) and the silt layers (2). Striations observed on the fault plane indicate pure reverse movement. The minimum vertical displacement along fault II is about 40 cm. The undisturbed units 3 and 3A overlie the whole faulted sequence.

3.1.3.1.2 Dating of the stratigraphic section. One sample of paleosol 1bA was dated using the ^{14}C method (Fig. 7) and provided a ^{14}C-calibrated age of 7540–5640 years B.C. (Table 1).

Dating the ceramic fragments collected from the same layer was difficult, due to their small size and absence of characteristic ornaments. Nevertheless, the colour and preparation technique allowed Dr. Rouben Badalian and Dr. Pavel Avetissian from the Institute of Archaeology and Ethnography of the National Academy of Sciences of Armenia to estimate an age of 4000–2000 years B.C.

Table 1
Ages calculated from the ^{14}C analysis of charcoal and paleosoil

Sample	Trench and unit	^{14}C age (years B.P.)	Calibrated years (B.P.)[a]	Calendar date (years B.C.)[a]	Material
only one	I; 1bA	7600±860	9490 (8390) 7590	7540 (6440) 5640	paleosoil
b	III; 4a	5930±330	7230 (6740) 6350	5280 (4790) 4400	charcoal
a	III; 3a	5410±420	6660 (6240) 5720	4710 (4290) 3770	charcoal
g	III; 3a	5270±740	6850 (5990) 5090	4900 (4040) 3140	charcoal
e	III; 2A	5030±170	5930 (5830) 5600	3980 (3880) 3650	paleosoil
f	III; 2A	4885±1225	7000 (5600) 3930	5040 (3650) 1980	charcoal
i	III; 3b	4735±470	5930 (5550) 4830	3980 (3600) 2890	charcoal
h	III; 3a	4340±70	5030 (4870) 4840	3080 (2920) 2890	charcoal
c, d	III; 4bA; 5A	2230±60	2340 (2200) 2150	390 (260) 200	paleosoil
only one	IV; 4A	3799±66	4280 (4170) 4090	2330 (2220) 2140	paleosoil
only one	V; 3A	6640±90	7600 (7540) 7430	5660 (5590) 5480	paleosoil

Data from Dr. J.L. Michelot (Laboratoire d'Hydrologie et de Géochimie Isotopique, Université de Paris Sud) for samples a, b, c, d, f, g, h, i, and, Dr. L.D. Sulergiski (Institute of Geology, Russian Academy of Sciences) for sample e taken by Prof. V.G. Trifonof.

[a] Ages in brackets are intercepts of calibrated ages (B.P. and B.C.). Maximum and minimum of calibrated age range (1σ) are indicated on each side of the value. Data calibrated using CALIB Rev. 4.3 (Stuiver and Reimer, 1993). Age ranges are rounded to the nearest decade.

3.1.3.1.3 Discussion and interpretation of events. We note the following:

• The fault scarp was eroded before the formation of the two upper units (3 and 3A).

• The northern fault (I, Fig. 7) that occurred before the formation of the paleosol (1aA–1bA) corresponds to a possible event older than 7540–5640 years B.C.

• Fault II (Fig. 7) was active after the formation of the silt unit (2) and before the formation of the modern soil (units 3–3A).

• The difference between the two ages—one based on archaeologically dated ceramics (Old Bronze age, 4000–2000 years B.C.) and the other on radiocarbon dating of the paleosol (7540–5640 years B.C.)—are consistent if one considers that the bulk dating of the soil provides an average age always older than that of burial. Moreover, the ceramics could have been deposited during the final stage of soil formation. Because the age of the ceramics has a large uncertainty, the age of the event is better constrained by ^{14}C (as maximum age), while the ceramic age provides a «possible better limit». Therefore, the most recent event occurred after 7540 years B.C. (from ^{14}C), and possibly after 4000 years B.C. (from ceramics), but before the time required to form horizons 3 and 3A of modern soil (age unknown). The interval of time required for the deposition of unit 2 cannot be estimated with the present constraints.

3.1.3.2. Trench III. Trench III was excavated on the southern slope of a ridge, located a few tens of meters NE of Trench I (Figs. 4 and 6). The trench is N–S oriented and crosscuts the main fault scarp (Vanadzor–Artanish fault segment). It was performed in two stages: a single slot trench was excavated and mapped in 1997 (Fig. 8), and the same trench was then widened and deepened (as a benched type) in 1998 (Fig. 9).

3.1.3.2.1 Stratigraphy, sedimentary environment and structures. Trench III provides abundant paleoseismologic information. The main fault plane is clearly visible and trends N100°E. Several layers containing various objects, such as ceramics with characteristic ornaments, a fireplace, obsidian tools, bones and charcoal, allowed dating by different methods (archaeological and C-14).

We have distinguished 12 main units (Figs. 8 and 9) and reached the base of the colluvial sequence. The units are from bottom to top:

(1) Fractured Cretaceous limestone, sometimes brecciated and strongly weathered (1a). A coating of hydrothermal minerals gives an ochre colour to the rock. It becomes more noticeable near fractures and the fault plane.

(2) Yellow silt with bluish lens (sag-pond deposit). The base contains blocks of fractured limestone. Between the blocks, wide calcite crystallisa-

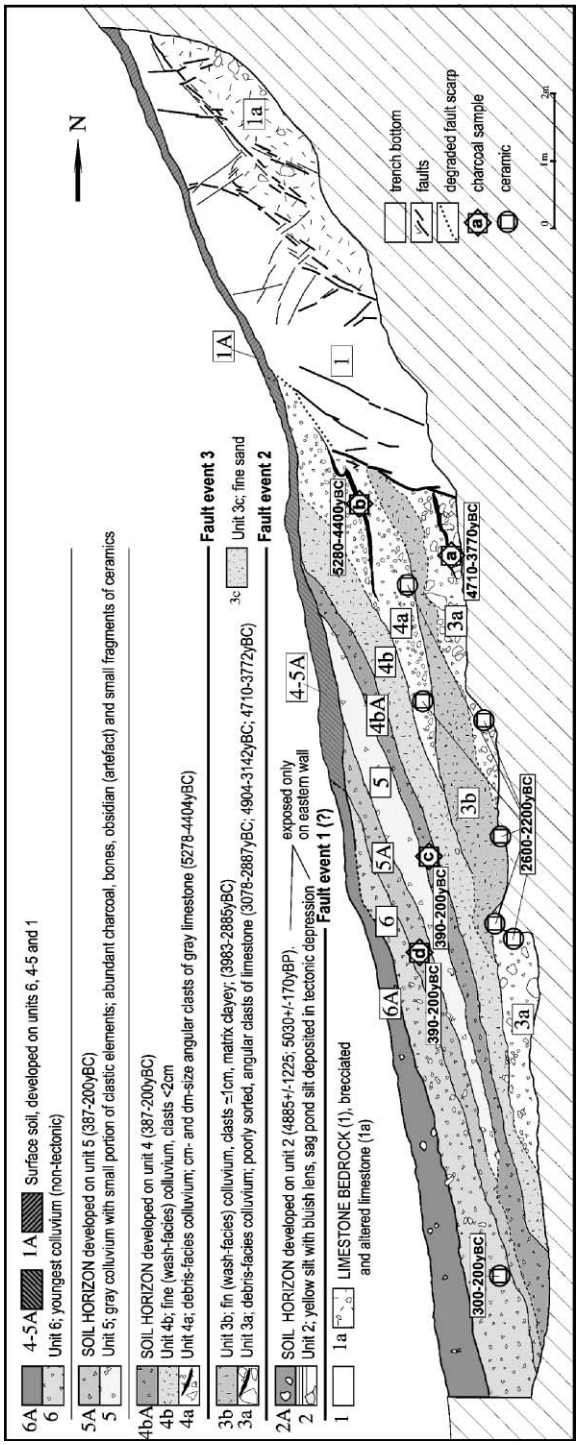

Fig. 8. Log of the western wall of Trench III.

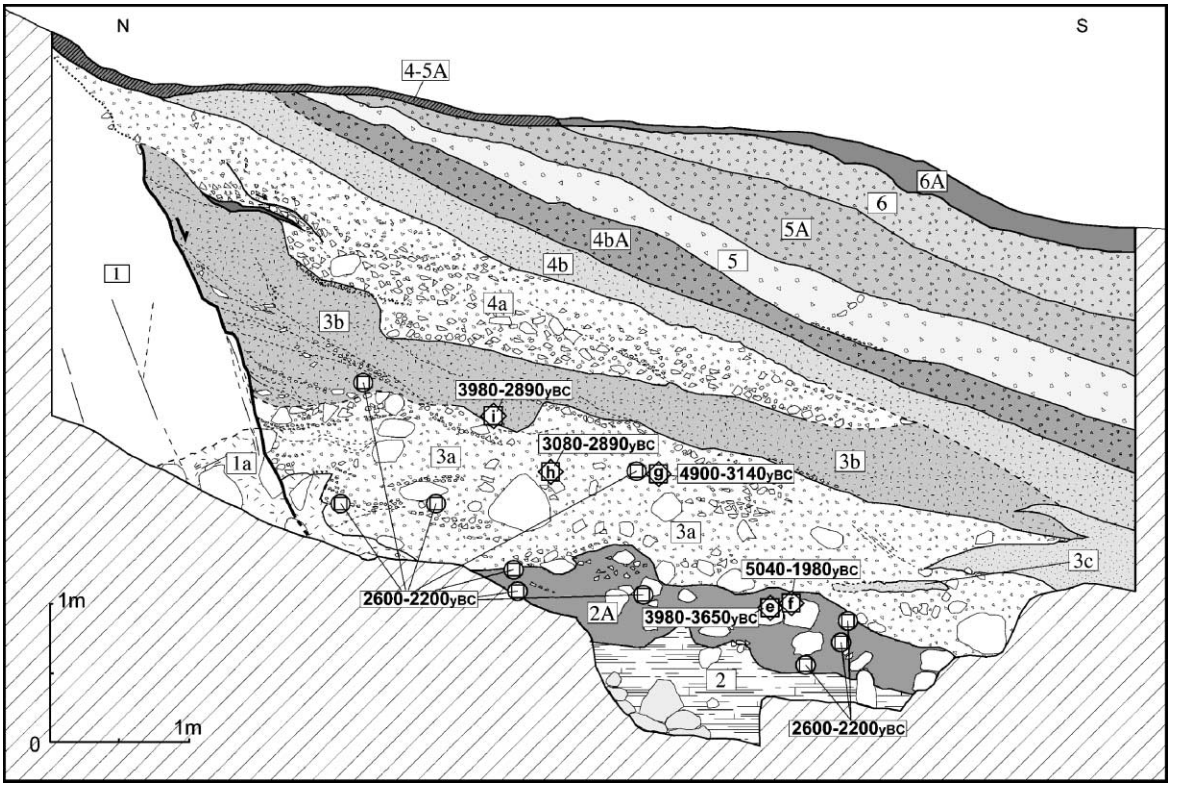

Fig. 9. Log of the western wall of Trench III.

tion is observed (the thickness can reach up to 11 cm).

(2A) Thick layer of dark paleosol containing large-size clasts (up to 20 cm). The matrix contains abundant organic fractions and charcoal (several large pieces, Fig. 9, samples e and f). This layer also contains large ceramic fragments. The soil formation is associated with human activity. One fireplace discovered at the base of the trench is probably contemporaneous with the paleosol.

(3a) Detrital formation of heterometric and angular clastic elements of limestone. Several big blocks (up to 50 cm in diameter) were discovered during the excavation. The overall fabric is chaotic, but it becomes more finely textured upwards. The sandy and less compacted matrix contains organic fractions. This unit displays centimetre-sized ceramic fragments and charcoal (Fig. 9, samples g and h). The latter is particularly abundant in 1- to 2-cm-thick lens (Fig. 8, sample a) and progressively disappears away from the scarp.

(3b) Homometric, centimetre-sized fine pebbles, ochre in colour due to hydrothermal alteration of limestone of the bedrock, with abundant clayey matrix derived from the altered bedrock of the foot wall. It is finely stratified near the fault plane. To the south, this unit progressively grades into a colluvium, whose matrix contains abundant organic fractions and charcoal (Fig. 9, sample i). No ceramic fragments were observed.

(3c) Fine sand of dark grey colour. This unit does not contain any charcoal or ceramic fragments. It is not sourced from the slope on the scarp, but rather associated with drainage flowing along the scarp.

(4a) Large clastic elements (centimetric and decimetric) of light grey limestone. This unit is poor in matrix and displays minor compaction. Upwards, the elements become finer. The unit contains centimetre-sized ceramic fragments and charcoal lenses that progressively disappear away from the scarp (sample b, Fig. 8).

(4b) Fine colluvium (less than 2 cm in size) with abundant matrix of dark colour. There are no ceramics in this layer.

(4bA) Black Paleosol developed on top of unit 4b, containing an abundant organic fraction and charcoal (Fig. 8, sample c), and few clastic elements.

(5) Grey colluvium containing a small fraction of clastic elements, abundant charcoal, bones, obsidian and small fragments of ceramic, and several stones and pebbles.

(5A) Light grey paleosol, containing abundant organic fractions and charcoal fragments (Fig. 8, sample d).

(6) Youngest colluvium, containing organic fractions, few centimetre-sized clastic elements and several small pottery fragments.

(6A) Modern soil (also 4–5A and 1A).

3.1.3.2.2 Dating of the stratigraphic section. Trench III shows numerous layers containing organic material, charcoal and ceramics. This has enabled the development of a chronological reference for the deposits exposed and to compare the results obtained with different dating techniques.

The ceramic fragments were dated at the Institute of Archaeology and Ethnography of the National Academy of Sciences, Armenia by Dr. Rouben Badalian and Dr. Pavel Avetissian. Ceramics present in units 2A, 3a; 3b and 4a belong to the Kura–Araxian culture of the Lower Bronze age (2600–2200 years B.C). The other ceramics (present in unit 6) date from the Late Antique epoch (Hellenistic, 300–200 years B.C.).

For the western wall, charcoal samples from units 3a (a) and 4a (b) (Fig. 8) were radiocarbon dated and provided calibrated ages of 5280–4400 years B.C. and 4710–3770 years B.C., respectively (Table 1). Two charcoal samples from two upper paleosol layers (c in 4bA and d in 5A in Fig. 8) were also dated. Samples c and d (Fig. 8) provided identical ages of 390–200 years B.C.

For the eastern wall (Fig. 9), the five charcoal samples e, f, g, h and i were dated and provided calibrated ages of 3980–3650, 5040–1980, 4900–3140, 3080–2890 and 3980–2890 years B.C., respectively (Table 1).

3.1.3.2.3 Discussion and interpretation.

3.1.3.2.3.1. Timing of events. The stratigraphic analysis has allowed us to make a number of hypotheses that are summarised in Fig. 10. We have distinguished a succession of colluvial wedges (each containing debris facies and wash facies) that could have been produced by two seismic events. The older colluvial wedge is composed of units 3a (debris facies) and 3b (wash facies), and the youngest wedge is composed of units 4a (debris facies) and 4b (wash facies). The clasts in lower debris facies (unit 3a) are larger than that in the upper debris facies (unit 4a). The transition from debris facies to wash facies is not abrupt, and reflects the gradual nature of free face degradation. The wash facies is stratified close to the fault plane. We emphasize that there is no soil layer between these two colluvial wedges, which attests that the deposition age of these units was close in time. Conversely, a soil unit is present (unit 4b) on top of the second wash facies (unit 4a).

Because the fault plane does not cut across the youngest colluvial wedge (unit 4a, Figs. 8 and 9), there has been no movement on this fault since the deposition of unit 4a. Therefore, units 5 and 6 are not interpreted as scarp-derived tectonic colluviums, but as superficial slope deposits. However, an even earlier seismic event is suggested by unit 2, which was probably deposited in a tectonic sag-pond.

The age of these events can be estimated (i) using age data for ceramics with characteristic elements, the fireplace, obsidians and charcoal, and, (ii) correlating these results.

As previously discussed, the majority of ceramics belong to the Kura–Araxian culture dated from 2600 to 2200 years B.C. This culture extends to the south and in the central part of the Caucasus, in Dagestan, in NW Iran and in the east of Anatolia. Radiocarbon dating of charcoal in units 2A, 3a and 3b provides an average age of 3500 years B.C., which is significantly older than the age bracket estimated for the ceramics. This may suggest a possible discrepancy of the Kura–Araxian culture age in this site.

Trenches II and III were excavated on the slope of the largest ridge (see Section 3.1.3) close to the village of Fioletovo (Fig. 4). An archaeological site was discovered on the top of the ridge. One outcrop situated above the trench site exposes several archaeological levels rich in various materials, including ceramics, bones, obsidian implements and abundant charcoal. The presence of ceramics with characteristic elements allowed archaeologists from the Institute of Archaeology and Ethnography of the National Academy of

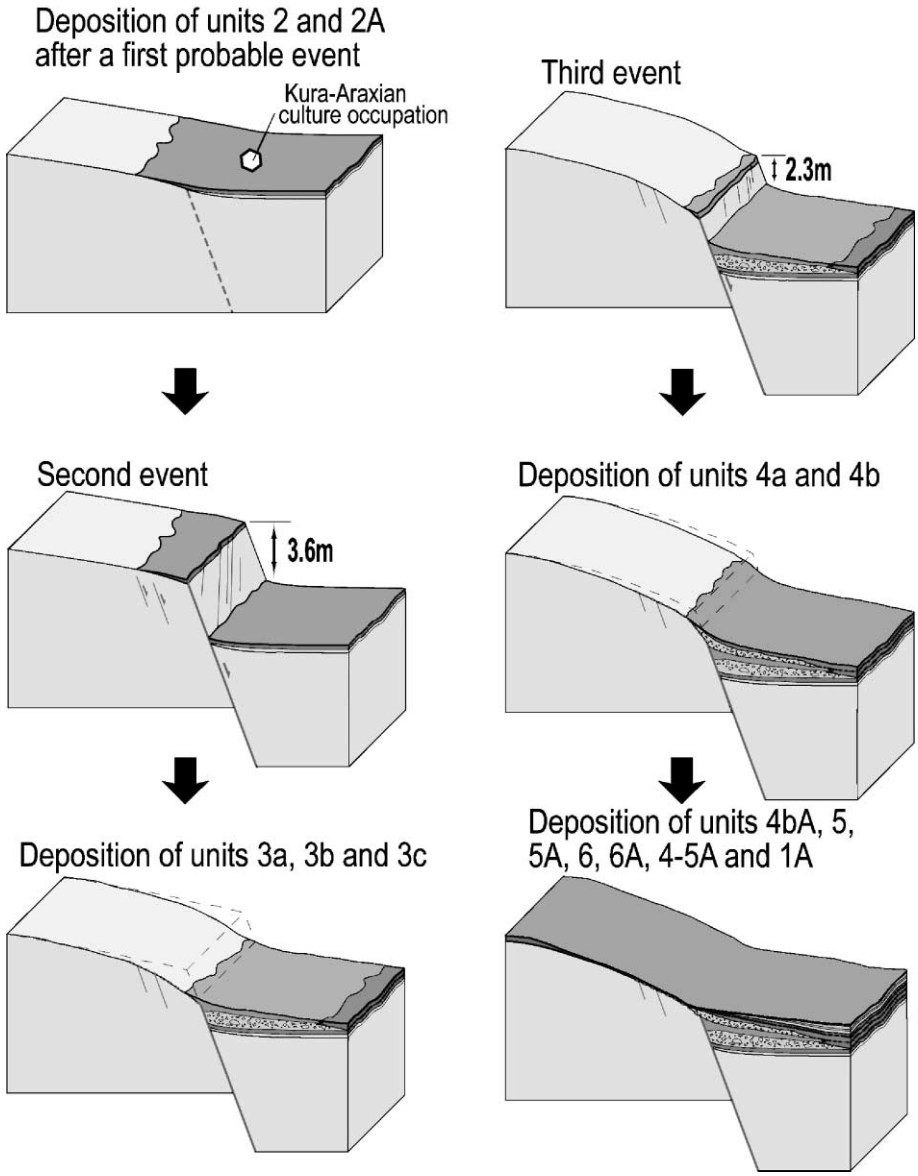

Fig. 10. Retrospective analysis of faulting events from Trench III, based on interpretation of units 3 and 4 as scarp-derived colluvial wedges. Units 5 and 6 do not contain debris facies, and unit 6 thickens away from the fault. They are therefore interpreted as non-tectonic colluvium.

Sciences to distinguish a last stage in the old Bronze Age (26th–22nd century B.C.) for the archaeological monument.

The dating of charcoal from two thin layers in units 3 and 4a shows no significant differences (a and b; Fig. 8). The charcoal from these two layers probably came from a single archaeological level, which outcrops a few meters above them, on the surface of the footwall (Fig. 7). This assumption is supported by the change in grain size of charcoal, which becomes smaller away from the scarp. This suggests a process of redeposition from upslope at the time of strong precipitation due to

charcoal's floatability. The same is true for the smaller sized ceramic fragments with smoothed broken edges. This may suggest that both the charcoal (sample h, 3080–2890 years B.C.) and the ceramic (2600–2200 years B.C.) are detritic in origin, and therefore predate the latest two seismic events.

The ceramic fireplace associated with large pieces of charcoal (samples e and f, Fig. 9 and Table 1) discovered on the lower paleosol (2A) was likely in situ. The ceramic fragments found in this unit are large sized and their broken edges are not smoothed. This implies that the ceramics was fragmented and remained in its original place. The ages of both ceramics and charcoal predate the last two seismic events represented by colluvial wedges.

From unit 4b upwards, including the two paleosol layers (4bA and 5A), all sedimentary sequences give evidence for slow depositional processes as they lay unconformably on the older units. This may be due to a change in the mode of sedimentation; from the detrital episode consistent with fault scarp degradation to the quiet inter-seismic period. The ceramics from unit 6 (300–200 years B.C.) and the C-14 age for paleosol layers 4bA and 5A (387–200 years B.C.) post-date the two latest seismic events (Fig. 8).

Therefore, both events took place between 3080 and 200 years B.C. (see also Fig. 18).

The archaeological site close to Trenches II and III on top of the hill is associated with copper metallurgy activity. This site had been occupied for several thousands of years by the Kura–Araxian culture. The fireplace that is cut by the fault in unit 2A (Trench III) is contemporaneous with this occupation. There is no evidence of Kura–Araxian culture in the site after 2200 years B.C. This suggests that the site has then been deserted until it was re-occupied by the culture of Low Iron Age after 1100 years B.C. On the other hand, the lower colluvial wedge (fault event 2) overlaps the Kura–Araxian archaeological paleosol 2A (Trench III). This suggests that desertion of the site was associated with this second seismic event, in the period close to 2200 years B.C. Because of the absence of soil between the two colluvial wedges, the third seismic event corresponding to the upper colluvial wedges (fault event 3) is close in time to the previous one.

3.1.3.2.3.2. Estimating displacements, magnitudes and slip rates. Deepening of the trench enabled us to reach the base of the older colluvial wedge (3a and 3b, Fig. 9) and to evaluate the cumulative vertical displacement of the two last fault events (events 2 and 3 in Trench III). Taking into account the facts that (i) Trench II is long but not deep, (ii) while Trench III is deep and short, and (iii) the two trenches are located only a few meters away from each other (no significant change in topography), we interpolated the data measured from these two trenches to evaluate the surface offset (Fig. 11a) after the two most recent events. We estimated the minimum surface offset at 5 m and the minimum vertical displacement at 5.6 m.

To estimate the vertical displacement associated with each event, we applied the «scarp degradation model» (initial scarp height = 2 × maximum colluvial thickness) proposed by McCalpin (1982). According to the «colluvial wedge model» (McCalpin, 1982, 1996), each surface rupture is followed by the formation of a discrete colluvial deposit and the number of fault-derived colluvial wedges should yield the number of seismic events. The colluvium volume must be comparable with that eroded from the scarp, and, therefore, it should be proportional to the amplitude of movement. The material incorporated in the colluvial wedge comes from the up thrown fault block (scarp-derived colluvium). If we take into account the portion of material from the upper part of the ridge and the degree of material compactness in the wedge, the volume of the colluvial wedge must be slightly higher compared to the volume of the degraded scarp (Fig. 11b).

Slope dip and climate play an important role in the process of sedimentation. A humid climate and moderate slope dip activate the erosion process, that is, scarp degradation. The sedimentation, activated by precipitation and the slope dip, results in thicker layers of colluvium. Alternatively, colluvium on a moderately inclined surface has a tendency to extend far from the scarp and to be deposited in thinner layers.

The vertical displacement corresponding to the lower colluvial wedge is of ca. 3.6 m [calculated by the scarp degradation model: maximum thickness of units (3a + 3b) × 2] and 2.3 m to the upper colluvial wedge [maximum thickness of units (4a + 4b) × 2] (see Fig. 9). The sum of 5.9 m is comparable to the profile-based estimate of 5.6 m (see Fig. 11).

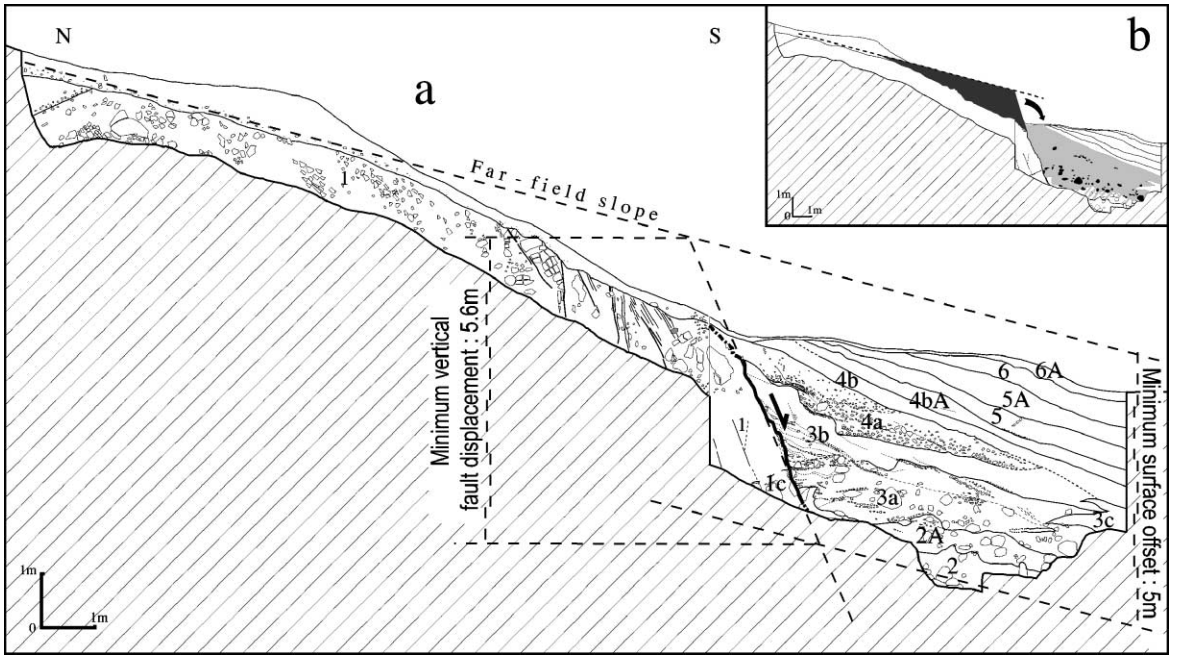

Fig. 11. (a) Surface offset, calculated by interpolation of logs of Trenches II and III after the last two seismic events; (b) scarp degradation: the volume of colluvial wedge is expected to be slightly higher compared to the volume of degraded scarp.

Therefore, we consider that the «scarp degradation model» (McCalpin, 1982) should be used with caution, not only for nearly horizontal surfaces, but also in the case of humid climatic zones with moderately inclined surfaces.

Taking into account the displacements calculated for both events and applying Wells and Coppersmith's (1994) regression curves, the magnitudes were estimated. Considering the complexity of the fault kinematics, the «all-slip-type equation» was used:

$$M = 6.93 + 0.82 \times \log(\mathrm{AD})$$

where M is the moment magnitude and AD is the average displacement.

The average displacement obtained from the position of the trench on the SW ridge flank was used. Morphology of the ridge and the scarp indicate that the measured values must be near to the average surface displacement. For event 2, we obtained a magnitude $M_w = 7.3$, and for event 3 a magnitude $M_w = 7.2$. If we consider the strike-slip component deduced from displaced morphologic features (see Section 3.1.2 and Fig. 3), we would have a magnitude $M_w > 7.3$ for the first individual earthquake and $M_w > 7.2$ for the second one.

The new results obtained from Trench III allow us to estimate the maximal slip rate along the Vanadzor–Artanich segment. The vertical cumulated displacement over 4200 years (since 2200 years B.C.) is 5.6 m. Moreover, assuming that the 30° rake of the fault measured a few kilometres west of the trench site and in Trench IV near Semionovka is the same (see Section 3.1.3.1), and having a horizontal displacement of 9.6 m, we can determine a slip rate of 2.28 mm/year. This estimation is consistent with the 2.24 ± 1 mm/year value calculated from the river offset (Section 3.1.2).

3.1.3.3. Trench IV. Trench IV, located 1.5 km east of the village of Semionovka (Fig. 5), was excavated in 1999. In this locality, the PSSF shows clear morphological evidence for recent activity. Trench IV is oriented N–S, perpendicular to the young and well-preserved scarp.

3.1.3.3.1 Stratigraphy and sedimentary environments and structures indicative of faulting events. A log of this trench is presented in Fig. 12. We have identified four main units ranging from the base to the surface:

(1a; 1b; 1c; 1d) Black (1a), yellow (1b), grey (1c) and light green plastic clay (1d).
(2) Light brown plastic clay to the base.
(2A) Paleosol developed in unit 2 with abundant organic fraction. The paleosol layer reaches a thickness of up to 80 cm. One fragment of weathered ceramic was present.
(2AB and 2B) Modern soil containing several centimetre-scale clasts.

Several fault planes dipping to the south are present. The dip of fault planes increases with depth, as in Trench IV. The northern fault cuts across the paleosol (2A) and is buried by the modern soil. A rake of 30° was measured on the fault plane.

3.1.3.3.2 Age of deposits. The paleosol sampled in the upper part of unit 2A (Fig. 12) was radiocarbon dated. An age of 2330–2140 years B.C. was obtained (Table 1). The altered piece of ceramic found in unit 2A was not datable.

3.1.3.3.3 Discussion and interpretation. A laminated structure, characterised by different colours, was observed in the southern part of the trench. The origin of these structures (units 1a–1d) is not clear, but they may be the result of hydrothermal alteration associated with the fault activity.

In the northern part of the trench, a south-dipping fault cuts across paleosoil 2A. The minimum vertical displacement (due to erosion after faulting) is 1 m. The geometry of striation observed on the fault plane allows us to calculate a minimum displacement of 2 m with a strike-slip component of 1.75 m. Applying Wells and Coppersmith's (1994) regression curves, we calculated a M>7.17 magnitude for the last fault event. This result is consistent with the magnitude calculated from Trench III in the Fioletovo site.

The paleosol sample provided a radiocarbon age of 2330–2140 years B.C. This age pre-dates the faulting event and strongly supports the hypothesis of an event at ca. 2200 years B.C. (Section 3.1.3.2.3), as previously discussed for the Fioletovo site.

3.2. The Khonarhasar site

3.2.1. Geologic and geomorphic setting of the site

The second area analysed in this study is located in the southeast of the Sevan Lake and is part of the Artanish–Sunik segment, also known as Khonarhasar segment (Figs. 2 and 13). The area is characterised by Neogene–Holocene volcanism that is present in the highest part of the Vardenis massif ($\sim$3000 m above sea level). The Neogene is represented by rhyolite-dacites, partly overlain by basaltic and andesitic-basaltic lava flows of the Lower and Middle Pleistocene (Karakhanian et al., 1997). The Holocene volcanism is represented by basalt flows that extend from the highest part of the massif to the Sevan lakeshore. The lava emission points are associated with the fault, which clearly shows the relationships between fault activity and volcanism. Volcanic cones, such as Khonarhasar, Tsursar (Fig. 13) and Porak (further to the southeast), are located along the fault that cuts across the Khonarhasar volcano with a dextral offset of 750±50 m (Figs. 13–15) and the Tsursar volcano with an offset of 350–400 m (Fig. 13). The eroded topography in older lava flows (i.e. 6.73±0.03 Ma, K–Ar radiometric age measured by P.Y. Gillot, Laboratoire de Géochronologie, Orsay) is also displaced. Indeed, ridges and streams are displaced by about 50 and 75 m, respectively (Fig. 13a and b). A recent lava flow (<20,000 years old) covers the trace of the fault in the south of Khonarhasar (Fig. 13), but a field survey shows that it is affected by the fault, as well. Several depressions of tectonic origin were formed (Fig. 13). They were created by shutter ridges with active sedimentation and are characterised by the presence of organic material.

3.2.2. An archaeological discovery indicative of faulting events

A vast zone of historical monuments (several districts belonging to different epochs, one town of the Bronze Age, a wall of many tens of kilometres, etc.) was discovered during our fieldwork (Philip and Karakhanian, 1999).

The fault crosscuts this archaeological site. In particular, it affects a Bronze Age wall that preserves a horizontal right lateral offset of about 1.80±0.2 m (Figs. 13c and 16). In detail, four sub-segments of the

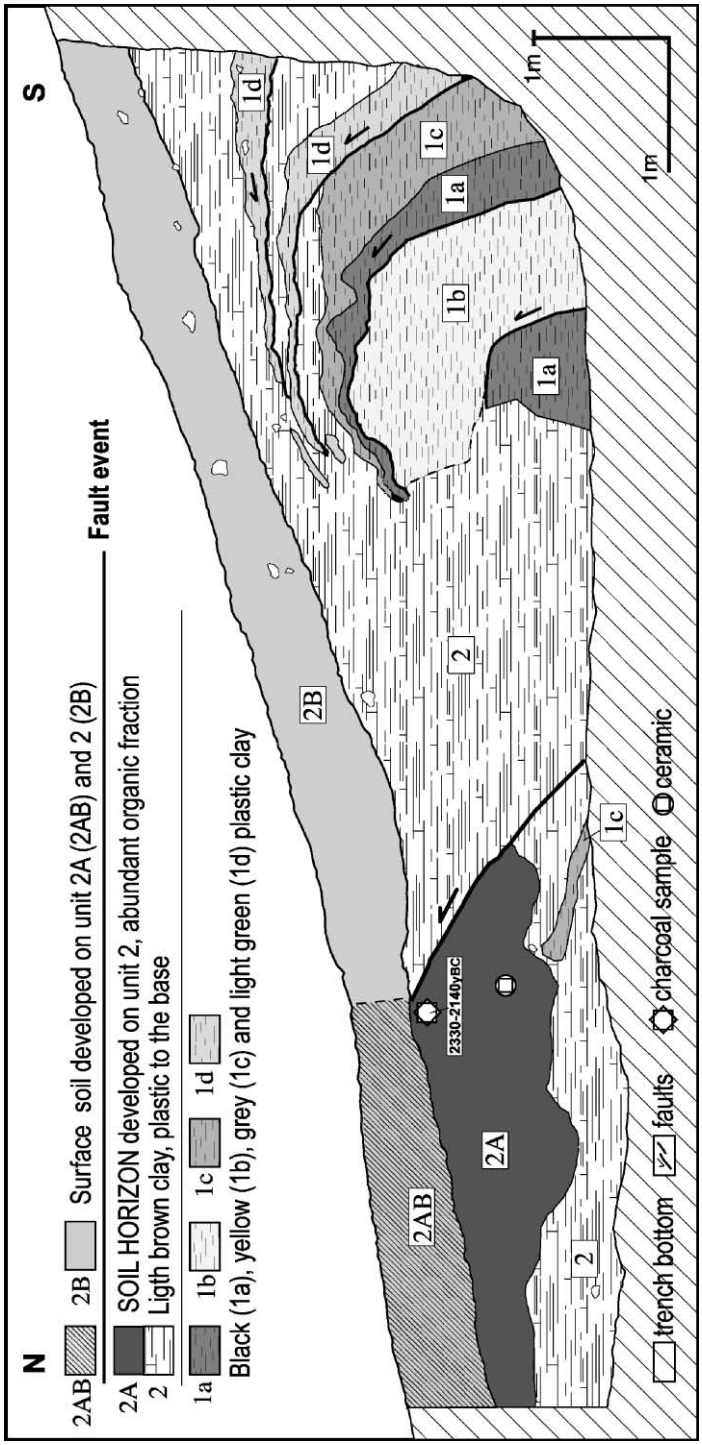

Fig. 12. Log of Trench IV.

Fig. 13. Detailed map of the Khonarhasar segment. (1) Recent lava flow; (2) archaeological site (Behoura); (3) endorheic basins; (4) faults; (5) offset volcanoes; (a) offset ridge; (b) offset river; (c) displaced wall; (d) site of Trench V.

fault affect the wall. A vertical component of displacement (ca. 80 ± 10 cm) was also noted. This pre-Urartian (Bronze Age) large city is a considerable archaeological monument that occupies several hectares in the vicinity of a number of very recent volcanoes (less than 15 km). These facts suggest that this city may be the one mentioned in the Arghishti's script, namely, the Behoura the Khorkhor cuneiform script of Arghishti, the Urartian king, discovered near the Van City (eastern Turkey) tells about a military campaign within the Sevan Lake region in 782–773 B.C. (Ohanessian and Abramian, 1981). That conquest may have been facilitated by geological phenomena, as suggested by the script that describes the conquest of the fortified Behoura City:

> By the grandeur of Khaldi, Arghishti says. . .When I encircled the (city) of Behoura once again

(repeatedly), Bam (or Bamni) mountain in the area of Behoura (city) was ruined. . .The smoke (and) soot from the city now rise to the sun. At the time the Bam (mountain) was destroyed, I took the city of Behoura.

This geological event could have also occurred in the region at 782–773 years B.C. It is assumed that a strong seismic event accompanied the eruption of the Porak volcano at that time (Philip and Karakhanian, 1999). This is consistent with the comments given in Ohanessian and Abramian's (1981) "Reader-Book of the Armenian People's History". A similar phenomenon also occurred further south (and was described) for the formation of the Sunik pull-apart in the PSSF (Karakhanian et al., 1997). The event described above might have taken place concurrently with the offset of the wall in the city of Behoura.

3.2.3. Slip rate estimation

Geologic, geomorphic and archaeological data allowed for an estimate of the slip rate along the Khonarhasar segment to be made.

The fault crosscuts the Khonarhasar volcano with a dextral offset of 750 ± 50 m (Figs. 14 and 15). About 6.5 km to the southeast, the same fault also crosscuts the Tsursar volcano that displays a dextral offset of 350–400 m (Fig. 13).

K–Ar dating of the Khonarhasar volcano provides an age of 1.4 ± 0.03 Ma (after P.Y. Gillot, Laboratoire de Géochronologie, Orsay). According to the division rule for values with unequal standard deviations (Geyh and Schleicher, 1990), we obtained a minimum slip rate of:

$$D/t = 750 \pm 50 \text{ m}/1400 \pm 30 \text{ Ka}$$

$$= 0.5367 \pm 0.0472 \text{ m/Ka}$$

$$\approx 0.53 \pm 0.04 \text{ mm/year}$$

Alternatively, the Bronze Age wall, affected by the fault as previously described, indicates a dextral offset of about 1.80 ± 0.2 m (Figs. 13c and 16). This offset was probably produced by the last major seismic event on this segment of the fault. Taking this into account, we can calculate the maximum (because the event is the last) horizontal slip rate by dividing the wall displacement value by the average age of the event (782–773 years B.C.). We obtained a maximum value of 0.64 ± 0.07 mm/year, which is slightly larger than the slip rate calculated from the Khonarhasar volcano displacement (0.53 ± 0.04 mm/year).

Assuming that the wall offset due to the last event is 1.80 ± 0.2 m horizontally and 80 ± 10 cm vertically, the oblique displacement would be 1.97 ± 0.05 m. According to Wells and Coppersmith's (1994) empiri-

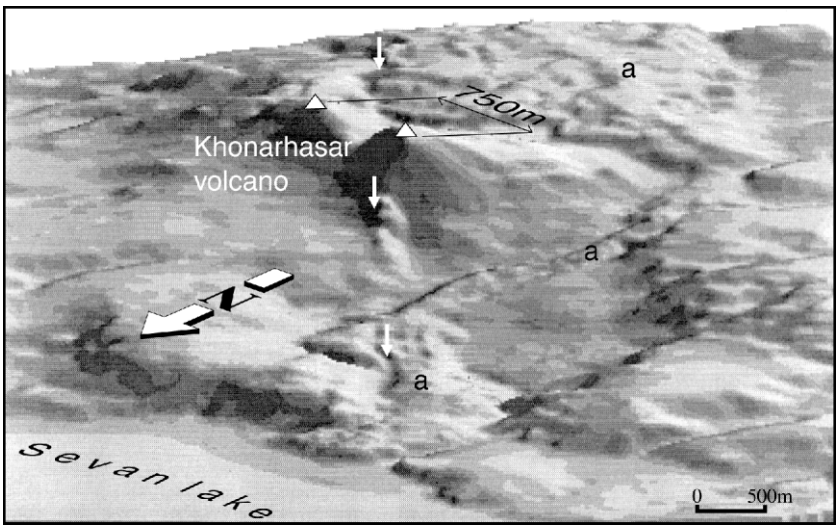

Fig. 14. Digital terrain model of the site with the displaced Khonarhasar volcano; a is recent lava flow. White arrows indicate the fault trace.

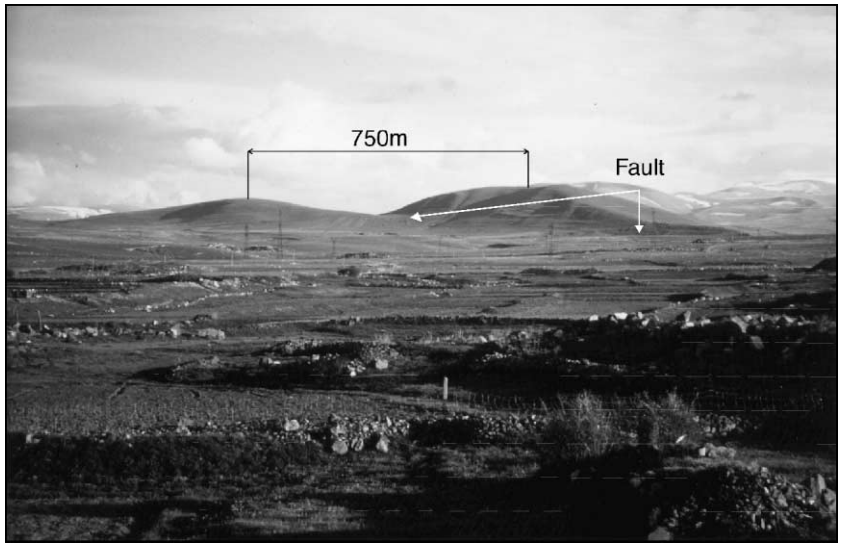

Fig. 15. The Khonarhasar volcano, displaced of ca. 750 m (view from the north).

cal relation and taking into account the above average displacement, a magnitude $M_w \geq 7.2$ was obtained for the last surface-breaking earthquake.

3.2.4. Paleoseismological investigation

Trench V was excavated perpendicular to the fault trace on the Khonarhasar segment. It is located near

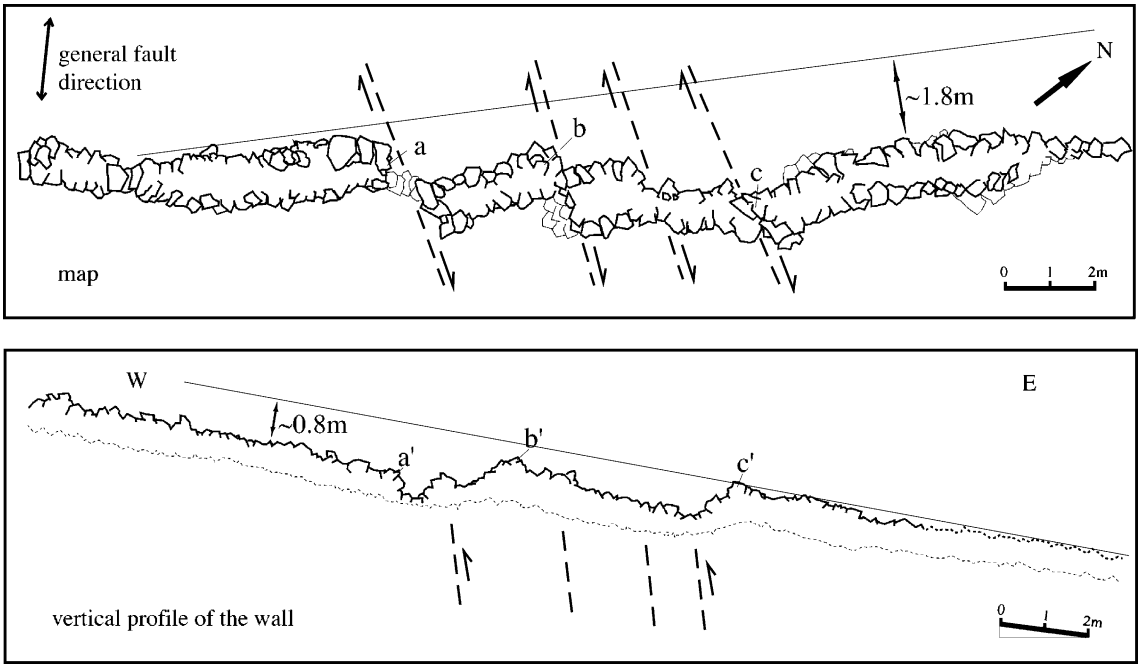

Fig. 16. Map and vertical profile of the displaced wall in the Behoura archaeological site.

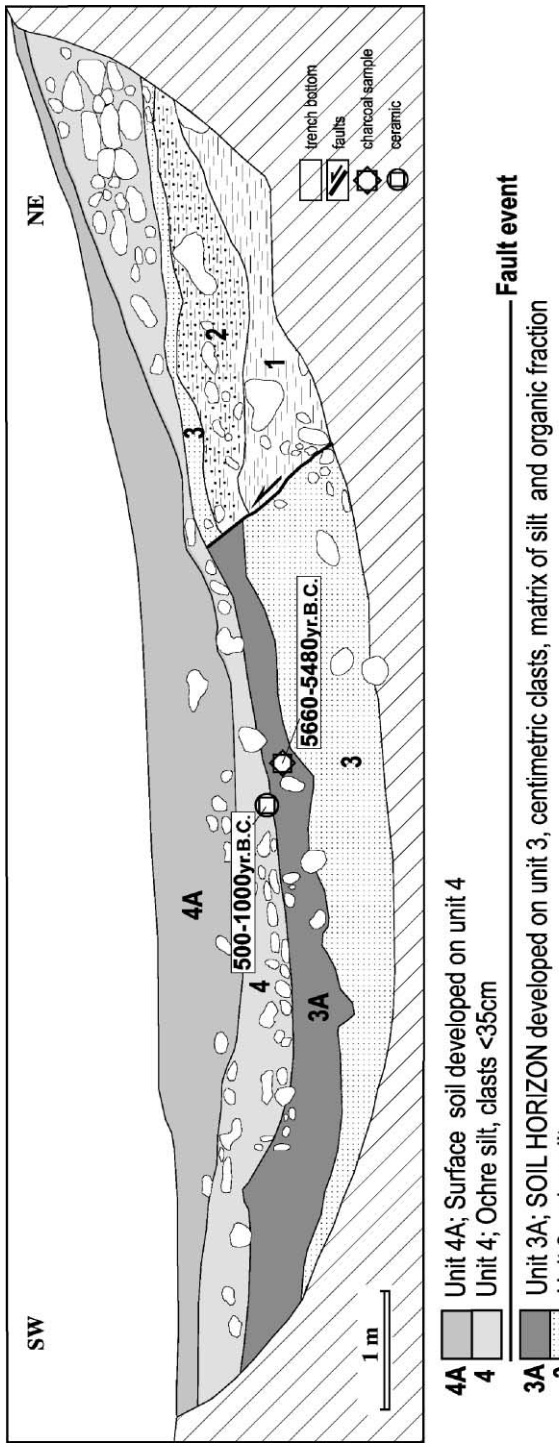

Fig. 17. Log of Trench V.

the Tsursar volcano (Fig. 13d) and contains stratigraphic evidence for a single seismic event.

3.2.4.1. Stratigraphy and sedimentary environments and structures indicating faulting events. From base to top, six main units were identified in Trench V (Fig. 17):

(1) Yellow, plastic compact clay, containing several clastic elements ranging in size from several millimetres to 40 cm.

(2) Colluvial clay, containing numerous small (several millimetres in size) and several large (5–50 cm in size) clastic elements.

(3) A layer of ochre silt, containing several small clastic elements close to the scarp.

(3A) Paleosol developed in unit 3 containing centimetre-sized, 20- to 60-cm-thick clasts. The matrix of this unit consists of silt with an abundant organic fraction.

(4) Ochre silt reaching a thickness up to 70 cm away from the fault, but becoming thinner (5–6 cm) closer to it. Numerous large clastic elements are mainly concentrated near the scarp. This unit could be interpreted as a colluvial wedge that was deposited in response to a surface rupture, along a fault that probably lies northeast of the end of the trench. This fault, associated with the topographic scarp, could be the main fault. In this case, the fault that is exposed in the trench and has no topographic expression would be subsidiary. Ceramic fragments are present at the base of this unit.

(4A) Modern soil.

The fault that is observed in the trench and shows an apparent reverse movement, cuts across the paleosol (3A) and the ochre silt (3) units. A minimum vertical displacement of 1.1 m has been estimated from the offset of the silt unit (3) exposed in the trench. We could not find any striations on the fault plane.

3.2.4.2. Timing of the event. Due to the lack of characteristic features, ceramics discovered at the base of unit 4 could not provide a precise age estimation. Nevertheless, archaeologists consider that an age of 500–1000 years B.C. is most likely. Organic material was also sampled for radiocarbon analysis. One sample from paleosol 3A gave an age of 5660–5480 years B.C. that pre-dates the faulting event. The major part of unit 3 and paleosol 3A in the hanging wall were eroded after the fault event, suggesting that part of the paleosol, and perhaps younger formations in the footwall, have also been eroded. As a consequence, the fault event may have occurred after 5660 years B.C. The archaeological age of the ceramics does not allow the faulting event to be dated precisely, because the ceramic fragments could have been reworked.

3.2.4.3. Discussion and interpretation. In Trench V, we observed a single event. The position of the base of silt unit 3 enables the determination of an apparent minimum vertical displacement (1.1 m). Former studies (Rebaï et al., 1993; Karakhanian et al., 1996), as well as the present one (displaced volcanoes, ridge, stream, wall and the striation in the basalt), show that the strike-slip component is largely dominant compared to the reverse one. All studies suggest that the average co-seismic slip per event on the fault is greater than 1.5 m (1.1/sin45°). Applying the Wells and Coppersmith's (1994) empirical equation for strike-slip faults for an average displacement of 1.5 m, a magnitude $M_w \geq 7.19$ can be calculated. Assuming a rake of movement of 24° as estimated from the displacement of the wall of Behoura (1.8 ± 0.2 m horizontal and 0.8 ± 0.1 m vertical) and a vertical displacement of 1.1 m, we obtained a horizontal component of about 2.4 m, which corresponds to an earthquake of magnitude $M_w = 7.3$. This particular earthquake would have occurred after the paleosoil formation and shortly before the formation of the unit 4 colluvial wedge.

The faulting event that displaced the wall in the Behoura archaeological site at 782–773 years B.C. and the event associated with the colluvial wedge that displaced the paleosol in Trench V probably correspond to the same event. The vicinity of the trench site and Behoura City (6.5 km) supports this conclusion (i.e. an earthquake of magnitude $M \geq 7.2$ corresponds to a surface rupture of ca. 65 km in length).

4. Discussion and conclusion

The small territory of the Republic of Armenia is characterised by a relatively high concentration of active fault zones that mainly correspond to large strike-slip faults. The slip rates on such faults are relatively small (less than 1 cm/year), and because the recurrence interval of large earthquakes is longer than

the period covered by historical documentation (despite the 2000 years record of historical seismicity in Armenia), it is difficult to characterise the fault activity without including paleoseismological investigations. The paleoseismological, archaeo-seismological and neotectonic studies that we undertook allowed us to estimate slip rates and recurrence intervals of large earthquakes along one of the largest active faults in Armenia: the PSSF. Paleoseismic investigations along the PSSF have permitted to characterise its recent faulting activity along two of its segments: the Vanadzor–Artanish and the Artanish–Sunik (Khonarhasar) segments.

Trenching on the Vanadzor–Artanish segment (Fioletovo and Semionovka sites, Trenches I; III and IV) displayed evidence for three large seismic events (Fig. 18). An earlier hypothetical seismic event (first) suggested by sag-pond deposits (unit 2) at the bottom of Trench III (before 4400 years B.C.) could correspond to the earthquake evidenced in Trench I (older than 5640 years B.C.). Two well-documented large events (second and third) occurred after this, between 3080 and 200 years B.C. (Trench III). It is considered that (i) desertion of the Fioletovo site can be associated with event 2, thus in the period near 2200 years B.C., and that (ii) seismic event 3 (Trench III) is close in time to event 2. The results (^{14}C dating age of 2333–2139 years B.C.) obtained from Trench IV strongly support the hypothesis of an event close to 2200 years B.C. The following period (about 4000 years), considered as the elapsed time, represents the last minimum recurrence interval.

Slip rates for the Vanadzor–Artanish segment, estimated from uplifted valley (see Section 3.1.2), are 1.28 ± 0.55 mm/year for the vertical component of the movement and 2.22 ± 0.95 mm/year for the horizontal component. This estimation of the horizontal slip rate is in agreement with the value of 2.28 mm/year calculated from Trench III data.

In the Khonarhasar segment, Trench V has allowed us to identify a single seismic event (Fig. 17). Evidence for this event is shown by (i) the offset of a Bronze Age wall (see Section 3.2.2) within an archaeological site that probably corresponds to the old Behoura City, and (ii) a faulting event observed in Trench IV (see Section 3.2.4). This faulting event could be associated with the 782–773 years B.C. historical event.

The 1.8 ± 0.2 m horizontal offset of the Bronze Age wall implies a maximum slip rate (because it is the final faulting event) of 0.64 mm/year. On a different time scale, the Khonarhasar volcano (1.4 ± 0.03 Ma) displays a horizontal offset of 750 ± 50 m (see Section 3.2.3). This implies a long-term slip rate of 0.53 mm/year. No creep was identified on this fault segment. The slip rate discrepancy between the Vanadzor–Artanish (2.24 ± 1 mm/year) and Khonarhasar segments (0.53–0.64 mm/year) may be explained by the fault zone splitting in two branches in the Artanish region, thus inducing a decrease of the rates southeasterly of the Artanish Peninsula (Fig. 2).

Having only one seismic event, we attempted to obtain indirect information on the recurrence intervals of large earthquakes in this part of the fault zone by using the following equation (Wallace, 1970):

$$\mathrm{RI} = D/S$$

where RI is the recurrence interval, D is the displacement during one event, and S is the coseismic slip rate. For the Khonarhasar segment, considering that a 1.8 ± 0.2 m horizontal displacement (offset of the Bronze Age wall) is associated with a single seismic event and having a 0.53 ± 0.04 value for the long-term slip rate, we obtained a recurrence interval of 3444 ± 637 years. In that case, the 750-m offset of the Khonarhasar volcano would correspond to nearly 406 seismic events in 1.4 Ma.

Comparing the results of the Fioletovo and Semionovka areas with that of the Khonarhasar area (Fig. 18), we concluded that three seismic events (including the first hypothetical event) occurred along the Vanadzor–Artanish segment and only one took place along the Artanish–Sunik segment.

Among several possible scenarios, two appear more realistic and are outlined below (Fig. 19):

(1) A first possible fault event occurred before 5640 years B.C. It was only observed in the Vanadzor–Artanish segment at Fioletovo (Trenches I and III). The second fault event (M>7.3) occurred approximately at 2200 years B.C. Evidence for this event was observed at both Fioletovo (Trench III) and Semionovka (Trench IV) in the same segment. Evidence for a third earthquake (M>7.2), close in time to the previous one, is present only at Fioletovo (Trench III). The last fault event took place in 782–

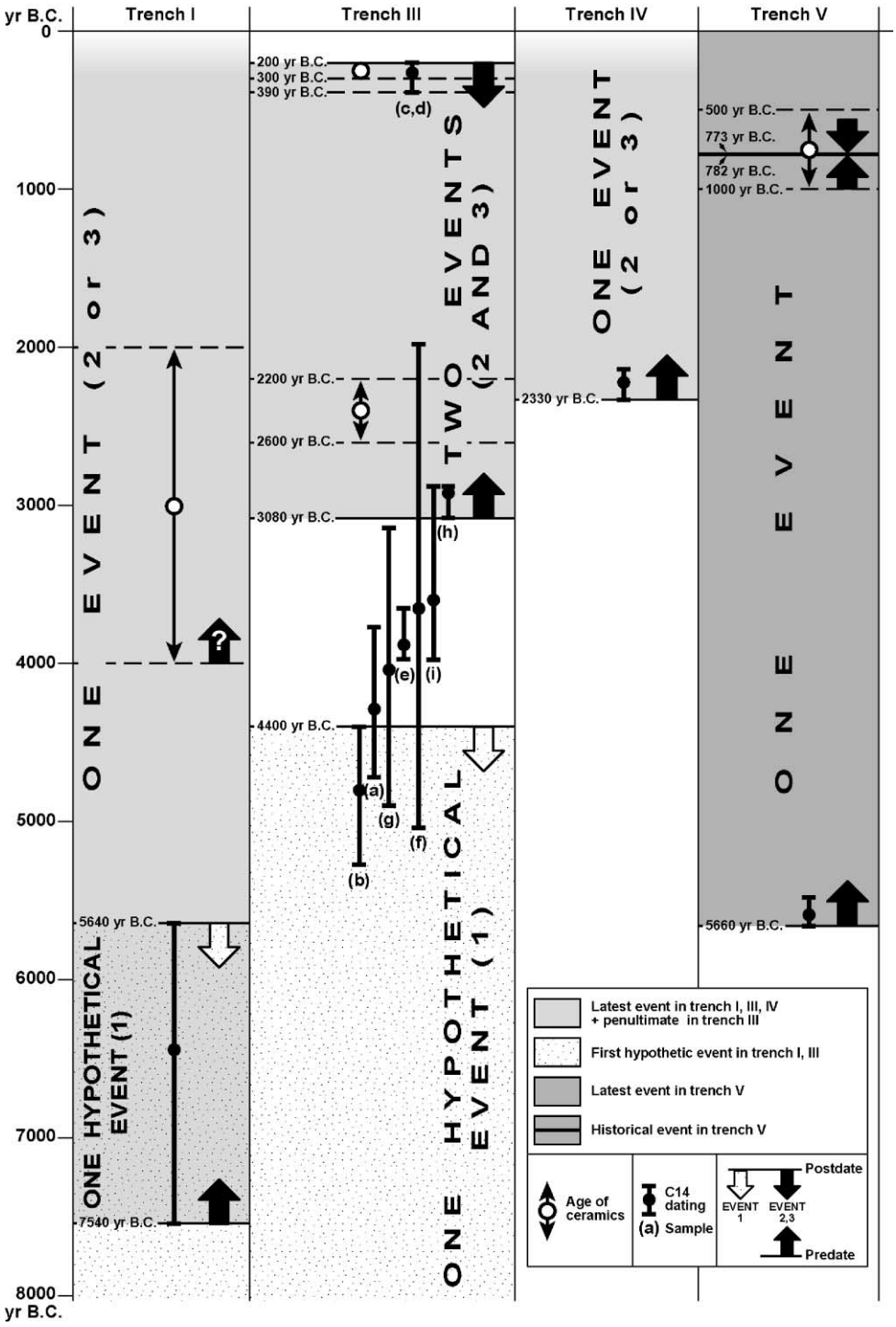

Fig. 18. Synthetic diagram of data in Trenches I, II, IV, and V. Summary of seismic events and age constraints.

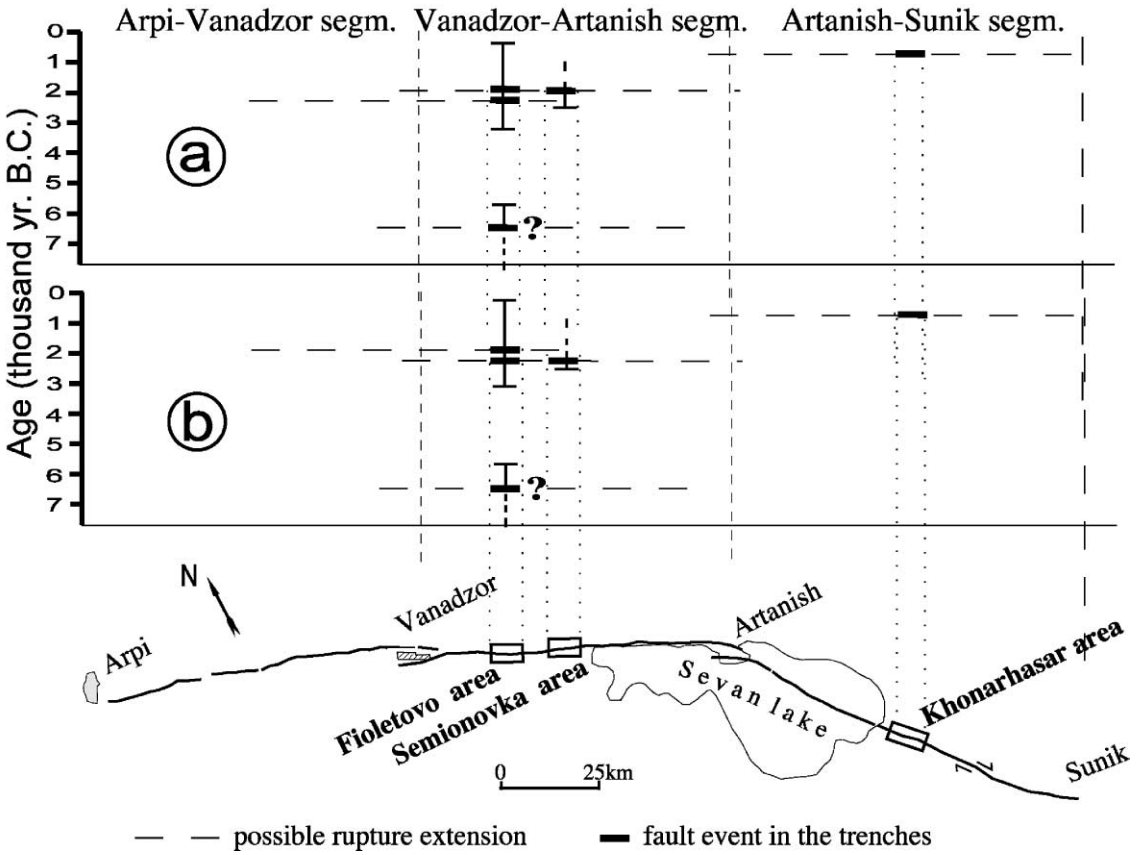

Fig. 19. Two scenarios of faulting events along the PSS fault zone for the last 9000 years.

773 years B.C. at Khonarasar in the Artanish–Sunik segment (a; Fig. 19).

In this scenario, the third fault event, seen in the site of Fioletovo, must extend to the west along the Arpi–Vanazor segment. This is a realistic hypothesis, because a fault cannot generate two large events along the same segment in such a short time interval. Similar patterns are consistent with (i) the sequential seismic activation in a short time interval, and (ii) the overlap of surface ruptures that were described along the North Anatolian fault zone for the 1666–1668 earthquakes, as well as for the 01/02/1994 and 13/08/1951 events (Barka, 1996).

(2) In the second scenario, the only difference concerns the second and third fault events. Indeed, the second event is observed only in the Fioletovo site in Trench III (M>7.3), while the third faulting event (M>7.2) is observed at both Fioletovo and Semionovka (Trenches III and IV). In this scenario, the second faulting event seen at the site of Fioletovo must have extended to the west along the Arpi–Vanazor segment (b; Fig. 19).

Additional data from elsewhere along the PSSF zone are still required to precisely estimate the extent of rupture and amount of displacement associated with each event. This is necessary to reconstruct any detailed model of long-term fault behaviour that can be useful and reliable for seismic hazard assessment. It is with this aim that we plan to excavate new trenches along other segments of the PSSF.

Acknowledgements

Funding via various grants (PICS-417, NATO ENVIR/LG grant 961097 and INTAS-0840) made

this study possible. We thank Dr. J.L. Michelot (Laboratoire d'Hydrologie et de Géochimie Isotopique, Université de Paris Sud) for providing the radiocarbon dating. We are grateful to Dr. R. Badalian and Dr. P. Avetissian (Institute of Archaeology and Ethnography, National Academy of Sciences of Armenia) for the analysis and dating of the ceramics. We are particularly indebted to Dr. J.P. McCalpin for his constructive criticisms that helped to improve this manuscript.

References

Ambraseys, N.N., 1988. Magnitude–fault length relationships for earthquakes in the Middle East. Historical Seismograms and Earthquakes of the World. Academic Press, San Diego, CA, United States, pp. 309–310.

Ambraseys, N.N., Adams, R.D., 1989. Long-term seismicity of North Armenia. Eos Trans. AGU 70, 145–154.

Ambraseys, N.N., Melville, C.P., 1982. A History of Persian Earthquakes. Cambridge Univ. Press, Cambridge, UK, p. 236.

Barka, A.A., 1996. Slip distribution along the North Anatolian fault associated with large earthquakes of the period 1939 to 1967. Bull. Seismol. Soc. Am. 86, 1238–1254.

Berberian, M., 1995. Master "blind" thrust faults hidden under the Zagros folds; active basement tectonics and surface morphotectonics. Tectonophysics 241 (3–4), 193–224.

Chase, C.G., 1978. Plate kinematics; the Americas, East Africa, and the rest of the world. Earth Planet. Sci. Lett. 37 (3), 355–368.

De Mets, C., Gordon, R.G., Argus, D.F., Stein, S., 1990. Current plate motions. Geophys. J. Int. 101, 425–478.

Dewey, J.F., Hempton, M.R., Kidd, W.S.F., Saroglu, F., Sengör, A.M.C., 1986. Shortening of continental lithosphere: the neotectonics of Eastern ANATOLIA—a young collision zone. Spec. Publ.-Geol. Soc. London 19, 3–36.

Geyh, M.A., Schleicher, H., 1990. Absolute Age Determination; Physical and Chemical Dating Methods and their Application. Springer, Berlin, Federal Republic of Germany, p. 503.

Jackson, J., 1992. Partitioning of strike-slip and convergent motion between Eurasia and Arabia in eastern Turkey and the Caucasus. J. Geophys. Res., B: Solid Earth Planets 97 (9), 12471–12479.

Jackson, J.A., McKenzie, D.P., 1984. Active tectonics of the Alpine–Himalayan Belt between western Turkey and Pakistan. Geophys. J. R. Astron. Soc. 77, 185–264.

Karakhanian, A.S., Djrbashian, R.T., Trifonov, V.G., Philip, H., Ritz, J.F., 1996. Active faults and strong earthquakes of the Armenian Upland. In: Giardini, D., Balassanian, S. (Eds.), Historical Earthquakes of Caucasus, pp. 181–188, ILP Publication No. 333, Kluwer Academic, Dordrecht.

Karakhanian, A.S., Trifonov, V.G., Azizbekian, O.G., Hondkarian, D.G., 1997. Relationship of late Quaternary tectonics and volcanism in the Khonarassar active fault zone, the Armenian Upland. Terra Nova 9, 131–134.

Ketin, I., 1948. Uber die tektonischmechanischen Folgerungen aus den grossen anatolischen Erdbeben des letzten Dezennimus. Geol. Rundsch. 36, 77–83.

Kostrov, B.V., 1974. Seismic moment and energy of earthquakes and seismic flow of rock. Izv. Acad. Sci. USSR, Phys. Solid Earth, Engl. Transl. 13, 13–21.

McCalpin, J.P., 1982. Quaternary geology and neotectonics of the west flank of the northern Sangre de Cristo Mountains, south-central Colorado. Colo. Sch. Mines Q. 77, 3.

McCalpin, J.P. (Ed.), 1996. Paleoseismology Academic Press, New York, 588 pp.

McKenzie, D.P., 1972. Active tectonics of the Mediterranean region. Geophys. J. R. Astron. Soc. 30, 109–185.

Minster, J.B., Jordan, T.H., 1978. Present-day plate motions. J. Geophys. Res. 83, 5331–5354.

Molnar, P., 1979. Earthquake recurrence intervals and plate tectonics. Bull. Seismol. Soc. Am. 69, 115–133.

Ohanessian, I., Abramian, A., 1981. Reader-Book of Armenian People's History, vol. 1, Izdatelsvo Lujs, Yerevan, Armenia.

Philip, H., Karakhanian, A., 1999. Tremblements de terre et archéologie. Pour la Science 261, 36–40.

Philip, H., Cisternas, A., Gvishiani, A., Gorshkov, A., 1989. The Caucasus: an actual example of the initial stages of a continental collision. Tectonophysics 161, 1–21.

Philip, H., Rogozhin, E., Cisternas, A., Bousquet, J.C., Borisov, B., Karakhanian, A., 1992. The Armenian earthquake of December 7, 1988: faulting and folding, neotectonics and paleoseismicity. Geophys. J. Int. 110, 141–158.

Rebaï, S., Philip, H., Dorbath, L., Borissoff, B., Haessler, H., Cisternas, A., 1993. Active tectonics in the Lesser Caucasus: coexistence of compressive and extensional structures. Tectonics 12 (5), 1089–1114.

Reilinger, R.E., Barka, A., 1997. GPS constraints on fault slip rates in Arabia–Africa–Aurasia plate collision zone: implications for earthquake recurrence times. In: Giardini, D., Balassanian, S. (Eds.), Historical and Prehistorical Earthquakes in the Caucasus. Kluwer Academic, Dordrecht, pp. 91–108.

Reilinger, R.E., McClusky, S.C., Oral, M.B., King, R.W., Toksoz, M.N., Barka, A.A., 1997. Global positioning system measurements of present-day crustal movements in the Arabia–Africa–Eurasia plate collision zone. J. Geophys. Res., B: Solid Earth Planets 102 (5), 9983–9999.

Sengör, A.M.C., Kidd, W.S.F., 1979. Post-collisional tectonics of the Turkish–Iranian plateau and a comparison with Tibet. Tectonophysics 55, 361–376.

Shebalin, N.V., Tatevossian, R.E., 1997. Catalogue of large historical earthquakes of the Caucasus. In: Giardini, D., Balassanian, S. (Eds.), Historical Earthquakes of Caucasus, pp. 201–232, ILP Publication No. 333, Kluwer Academic, Dordrecht.

Stuiver, M., Reimer, P.J., 1993. Extended 14C data base and revised CALIB 3.0 14C age calibration program. Radiocarbon 35, 215–230.

Taymaz, T., Jackson, J., McKenzie, D., 1991. Active tectonics of the north and central Aegean sea. Geophys. J. Int. 106, 433–490.

Trifonov, V.G., Karakhanyan, A.S., Kozhurin, A.I., 1990. The Spi-

tak earthquake as an expression of present tectonic activity. Geotectonics 24 (6), 505–515.

Vardaniants, L.A., 1948. The post-Pliocene history of the region of Caucasus–Black sea–Caspian sea. Izd. Natl. Acad. Arm. SSR, pp. 17–21.

Wallace, R.E., 1970. Earthquake recurrence intervals on the San Andreas fault. Geol. Soc. Am. Bull. 81 (10), 2875–2889.

Wells, D.L., Coppersmith, K.J., 1994. Empirical relationships among magnitude, rupture length, rupture area, and surface displacement. Bull. Seismol. Soc. Am. 84, 974–1002.